

Dynamical system analysis in multiscalar-torsion cosmology

Genly Leon,^{1,2,*} Andronikos Paliathanasis,^{2,1,†} and Alfredo D. Millano^{1,‡}

¹*Departamento de Matemáticas, Universidad Católica del Norte,*

Avda. Angamos 0610, Casilla 1280 Antofagasta, Chile

²*Institute of Systems Science, Durban University of Technology,*

PO Box 1334, Durban 4000, South Africa

(Dated: March 7, 2024)

We explore the phase-space of a multiscalar-torsion gravitational theory within a cosmological framework characterized by a spatially flat Friedmann–Lemaître–Robertson–Walker model. Our investigation focuses on teleparallelism and involves a gravitational model featuring two scalar fields, where one scalar field is coupled to the torsion scalar. We consider coupling in the two scalar fields’ kinetic and potential components. We employ exponential functions for the scalar field potentials and analyze the field equations’ equilibrium points to reconstruct the cosmological evolution. Remarkably, we discover many equilibrium points in this multiscalar field model, capable of describing various eras of cosmological evolution. Hence, this model can be used to describe the early and late time acceleration phases of the universe and as a unification model for the elements of the dark sector of the universe.

PACS numbers: 98.80.-k, 95.35.+d, 95.36.+x

Keywords: Teleparallel; Scalar field; Scalar-torsion; Dynamical analysis

1. INTRODUCTION

Recent cosmological observations suggest that our universe is currently experiencing acceleration [1–5], as well as having undergone a period of acceleration during its early stage

*Electronic address: genly.leon@ucn.cl

†Electronic address: anpaliat@phys.uoa.gr

‡Electronic address: alfredo.millano@alumnos.ucn.cl

known as cosmic inflation [6]. The early acceleration phase is attributed to the inflation [7], while dark energy is believed to be responsible for the late-time acceleration. Both dark energy and inflaton are fluid sources with negative pressure components that provide acceleration. A fascinating possibility is that these two eras of acceleration, inflation and late-time acceleration, may be interconnected. It is conceivable that dark energy and inflation arise from the same underlying physical mechanism, manifesting at different stages in the universe's evolution. However, a comprehensive theory needs to be revised to explain the connection between inflation and late-time acceleration, particularly considering the vast disparity in energy scales between these two phenomena.

The concept of cosmic acceleration is often explained through scalar fields. In the context of inflation, a scalar field with a nonzero mass term is assumed to drive the dynamics, resulting in an acceleration period during the slow-roll limit. Various potential functions for scalar fields have been proposed in the literature for inflation, as seen in references [8–14]. A review article, reference [15], provides a detailed list of these proposed inflationary models. The quintessence theory is a straightforward model for dynamical dark energy [16, 17]. This theory involves introducing an adjusting or tracker scalar field [18], which, while rolling down the potential function, can provide acceleration [19–26]. The quintessence model can also describe the degrees of freedom of other dark energy models, such as the Chaplygin gas fluids [27–29], to provide a unified description for the dark energy components of the universe [30, 31].

There are several proposed generalizations of scalar field models. One such generalization is the phantom scalar field [32–34]. In this model, the presence of a scalar field allows for the possibility of negative energy density. As a consequence, the equation of the state parameter can cross the phantom divide line. That leads to an accelerated universe expansion that exceeds the exponential growth predicted by the de Sitter solution, ultimately resulting in a cosmological singularity known as the Big Rip [35]. Another proposal to explain these phenomena is the chameleon theory, which suggests that the scalar field interacts with other matter components in the universe. This interaction gives rise to a chameleon mechanism, whereby the scalar field's properties change depending on the surrounding matter environment.[36, 37]. In this theory, the mass of the scalar field depends on the mass of the other matter components of the universe [38, 39].

Extensive research has been conducted on nonminimally coupled scalar fields, which

involve the interaction between the scalar field and gravity within the gravitational action integral. These are known as scalar-tensor theories of gravity [40] and include the Brans-Dicke theory as a particular case [41]. These theories are consistent with Mach's principle, which requires the existence of the scalar field. They are related to minimally coupled scalar field models by a geometric map that connects the Einstein and the Jordan frames through a conformal transformation [42]. However, the physical properties of a gravitational theory rarely survive this transformation [43, 44]. Other nonminimally coupled scalar field gravitational theories have also been proposed [45–49]. Multiscalar field models have also been studied extensively [50–53] as they provide new degrees of freedom to explain various eras of cosmological history and connect the early-time acceleration phase with the late-time acceleration [54].

Modified gravity theories offer alternative explanations for the universe's acceleration [55, 56]. These theories modify the Einstein-Hilbert Action by introducing geometric invariants in the field equations that provide acceleration through geometrodynamical terms. In General Relativity, the Ricci scalar R is the fundamental scalar constructed using the Levi-Civita connection. However, using a general connection, we can construct the non-metricity scalar Q and the torsion scalar T , which, along with R , are known as the trinity of gravity [57]. When the antisymmetric Weitzenböck connection is the fundamental connection of physical space [58], the torsion scalar T can be used as gravitational Lagrangian [59, 60], leading to the teleparallel equivalent of General Relativity. Introducing a nonminimally coupled scalar field results in a scalar-torsion theory [61–63], which differs from the scalar-tensor theory of gravity [64]. The scalar-torsion theory has been applied to describe the late-time acceleration of the universe in [65–68]. From the phase-space analysis of the field equations in scalar-torsion theory [69] it was found that the asymptotic solutions described by the quintessence scalar field or the phantom scalar field of General Relativity are provided. Additionally, the de Sitter point always exists. In [70], inflation in scalar-tensor theory was investigated. The analysis of the dynamics found that some asymptotic saddle points can be attributed to inflation. For a discussion we refer the reader to [71–75] and references therein.

A multiscalar field cosmology was recently explored in teleparallelism in [78]. In this model, one of the fields is coupled to the torsion scalar T through a diatonic coupling function, while the other field minimally couples to gravity. Still, there exists nonzero

interaction between the two fields. The field equations for the multiscalar field models are of second order, and the Noether symmetry analysis is used to determine exact and analytic solutions and specify the scalar field potentials.

This research examines the multiscalar-torsion theory in the publication by [78]. Our goal is to conduct a thorough phase-space analysis that will allow us to reconstruct the universe's history and evaluate the feasibility of the gravitational model proposed in [79]. This analytical approach has been widely utilized in various gravitational theories, as evident in the references [80–85]. Using phase-space analysis, we can effectively identify crucial epochs in cosmological history and draw insightful conclusions regarding the initial value problem. The paper is structured as follows.

Section 2 introduces teleparallelism's fundamental concepts and definitions. We also discuss our gravitational model, which involves two coupled scalar fields within scalar-torsion theory. Our primary focus will be on studying a spatially homogeneous cosmology, where we will derive the modified Friedmann equations for the Friedmann-Lemaître-Robertson-Walker metric tensor. To investigate the overall evolution of the physical parameters described by the modified Friedmann equations, we will introduce dimensionless variables and express the cosmological field equations as first-order algebraic-differential equations in Section 3. The novel contributions of this study are covered in Sections 4 and 5, where we present the equilibrium points of the field equations in both finite and infinite regimes. Each equilibrium point represents an asymptotic solution for the cosmological model. We will delve into the physical properties of these solutions and analyze their stability, as this information is crucial for understanding the cosmological evolution of the multiscalar-torsion model and addressing the theory's initial value problem. Finally, in Section 6, we will summarise our findings.

2. MULTISCALAR-TORSION GRAVITY

We work in the context of the teleparallel theory of gravity coupled to a scalar field. In particular, we consider the multiscalar field gravitational model with Action Integral [65]

$$S = \frac{1}{16\pi G} \int d^4x e \left[F(\phi) \left(T + \frac{\omega}{2} \phi_{;\mu} \phi^\mu + U(\phi) + L(x^\kappa, \phi, \psi, \psi_{;\mu}) \right) \right], \quad (1)$$

which belongs to the family of scalar-torsion theories.

Where in the Action Integral (1), ϕ is the scalar field nonminimally coupled to the torsion

scalar T , $F(\phi)$ is the coupling function between the scalar field ϕ and T , $U(\phi)$ is the scalar field potential, and $L(x^\kappa, \phi, \psi, \psi_{;\mu})$ describe the dynamics of a second-scalar field. $\psi_{;\mu}$ denotes the covariant derivative. Parameter ω is arbitrary, and its value reflects the coupling with gravity.

The torsion scalar T is defined by the antisymmetric Weitzenböck connection $\hat{\Gamma}^\lambda_{\mu\nu}$, that is,

$$T = S_\beta{}^{\mu\nu} T^\beta_{\mu\nu}, \quad (2)$$

in which $T^\beta_{\mu\nu}$ is the torsion tensor defined as

$$T^\beta_{\mu\nu} = \hat{\Gamma}^\beta_{\nu\mu} - \hat{\Gamma}^\beta_{\mu\nu}, \quad (3)$$

and

$$S_\beta{}^{\mu\nu} = \frac{1}{2}(K^{\mu\nu}{}_\beta - \delta^\mu_\beta T_\theta{}^{\theta\nu} + \delta^\nu_\beta T_\theta{}^{\theta\mu}), \quad (4)$$

where now

$$K^{\mu\nu}{}_\beta = -\frac{1}{2}(T^{\mu\nu}{}_\beta - T^{\nu\mu}{}_\beta - T_\beta{}^{\mu\nu}), \quad (5)$$

is the contorsion tensor. The Weitzenböck connection $\hat{\Gamma}^\lambda_{\mu\nu}$ is related to the vierbein fields $e_i = h_i^\mu \partial_\mu$, as $\hat{\Gamma}^\lambda_{\mu\nu} = h_a^\lambda \partial_\mu h_\nu^a + \omega^a{}_{\nu\kappa} h_\mu^\kappa h_a^\lambda$ with the metric tensor $g_{\mu\nu}$ to be defined as $g_{\mu\nu} = \eta_{ij} h_\mu^i h_\nu^j$, and $\omega^{\lambda}{}_{\nu\kappa}$ is the spin connection [76].

For the second scalar field we assume $L(x^\kappa, \phi, \psi, \psi_{;\mu}) = \frac{\beta}{2} \psi_{;\mu} \psi^{;\mu} + \frac{\hat{V}(\phi, \psi)}{F(\phi)}$, where now the Action Integral (1) reads [78]

$$S = \frac{1}{16\pi G} \int d^4x e \left[F(\phi) \left(T + \frac{\omega}{2} \phi_{;\mu} \phi^{;\mu} + U(\phi) + \frac{\beta}{2} \psi_{;\mu} \psi^{;\mu} \right) + \hat{V}(\phi, \psi) \right], \quad (6)$$

where $\beta^2 = 1$. We have introduced a new potential function $\hat{V}(\phi, \psi)$ in order to be able to introduce interaction between the two scalar fields ϕ and ψ . Parameters ω and β are nonzero parameters, and their values define the nature of the scalar fields.

Last but not least, we want to discuss that in order to end the latter Action (6) with starting point (1), we considered a specific representation for the scalar field; for more details, we refer the reader to the discussion in [77].

2.1. FLRW cosmology

In our analysis, we assume that the universe is described by the four-dimensional isotropic, homogeneous, and spatially flat FLRW (Friedmann-Lemaître-Robertson-Walker) geometry.

This assumption allows us to employ a specific line element to characterize the properties of the universe. Specifically, we select the metric tensor $g_{\mu\nu}$ with line element

$$ds^2 = -dt^2 + a^2(t)(dx^2 + dy^2 + dz^2), \quad (7)$$

where $a(t)$ is the scale factor.

Moreover, we consider the diagonal vierbein fields [65]

$$h^i{}_{\mu}(t) = \text{diag}(1, a(t), a(t), a(t)), \quad (8)$$

and the zero spin connection in Cartesian coordinates [76].

From the latter follows $T = 6H^2$, with $H = \frac{\dot{a}}{a}$, $\dot{a} = \frac{da}{dt}$, to be the Hubble function. For the latter vierbein fields, the limit of General Relativity is recovered when the dynamical components of the scalar fields are eliminated.

Thus, from (6) we calculate the point-like Lagrangian [78]

$$\mathcal{L}(a, \dot{a}, \phi, \dot{\phi}, \psi, \dot{\psi}) = F(\phi) \left(6a\dot{a}^2 + a^3 \left(\frac{\omega}{2}\dot{\phi}^2 + \frac{\beta}{2}\dot{\psi}^2 \right) - a^3 V(\phi, \psi) \right), \quad (9)$$

while the gravitational field equations are

$$6H^2 + \frac{\omega}{2}\dot{\phi}^2 + \frac{\beta}{2}\dot{\psi}^2 - V(\phi, \psi) = 0, \quad (10)$$

$$\dot{H} + \frac{3}{2}H^2 - \left(\frac{1}{4} \left(\frac{\omega}{2}\dot{\phi}^2 + \frac{\beta}{2}\dot{\psi}^2 + V(\phi, \psi) \right) - H\dot{\phi}(\ln(F(\phi)))_{,\phi} \right) = 0, \quad (11)$$

$$\ddot{\phi} + 3H\dot{\phi} + \frac{1}{\omega}(\ln(F(\phi)))_{,\phi} \left(\frac{\omega}{2}\dot{\phi}^2 - \frac{\beta}{2}\dot{\psi}^2 - 6H^2 - V(\phi, \psi) \right) - \frac{1}{\omega}V_{,\phi} = 0, \quad (12)$$

$$\ddot{\psi} + 3H\dot{\psi} + (\ln(F(\phi)))_{,\phi}\dot{\phi}\dot{\psi} - \frac{1}{\beta}V_{,\psi} = 0. \quad (13)$$

We have defined the function $V(\phi, \psi)$ such that $\hat{V}(\phi, \psi) = -V(\phi, \psi)F(\phi) - F(\phi)U(\phi)$.

In the following, we consider the coupling function $F(\phi) = F_0 e^{2\phi}$. That is not an arbitrary selection. For such a function, in the absence of the second-scalar field, the gravitational model admits an $O(d, d)$ duality symmetry and it has many similarities with the Brans-Dicke model of scalar-tensor theory [63, 64].

Therefore, for $F(\phi) = F_0 e^{2\phi}$ the gravitational field equations (10)-(13) read [78]

$$6H^2 + \frac{\omega}{2}\dot{\phi}^2 + \frac{\beta}{2}\dot{\psi}^2 - V(\phi, \psi) = 0, \quad (14)$$

$$\dot{H} + \frac{3}{2}H^2 - \left(\frac{1}{4} \left(\frac{\omega}{2}\dot{\phi}^2 + \frac{\beta}{2}\dot{\psi}^2 + V(\phi, \psi) \right) - 2H\dot{\phi} \right) = 0, \quad (15)$$

$$\ddot{\phi} + 3H\dot{\phi} + \frac{2}{\omega} \left(\frac{\omega}{2}\dot{\phi}^2 - \frac{\beta}{2}\dot{\psi}^2 - 6H^2 - V(\phi, \psi) \right) - \frac{1}{\omega} V_{,\phi} = 0, \quad (16)$$

$$\ddot{\psi} + 3H\dot{\psi} + 2\dot{\phi}\dot{\psi} - \frac{1}{\beta} V_{,\psi} = 0. \quad (17)$$

An equivalent way to write the field equations (14)- (15) is

$$3H^2 = \rho_{eff}, \quad (18)$$

$$2\dot{H} + 3H^2 = -p_{eff}, \quad (19)$$

where ρ_{eff} and p_{eff} are the components of the effective fluid defined by the two scalar fields as follows

$$\rho_{eff} = \frac{1}{2} \left(-\frac{\omega}{2}\dot{\phi}^2 - \frac{\beta}{2}\dot{\psi}^2 + V(\phi, \psi) \right), \quad (20)$$

$$p_{eff} = \left(\frac{1}{2} \left(-\frac{\omega}{2}\dot{\phi}^2 - \frac{\beta}{2}\dot{\psi}^2 - V(\phi, \psi) \right) + 4H\dot{\phi} \right). \quad (21)$$

The equation of state parameter for the effective fluid is defined as $w_{eff} = \frac{p_{eff}}{\rho_{eff}}$, that is

$$w_{eff} = \frac{\left(-\frac{\omega}{2}\dot{\phi}^2 - \frac{\beta}{2}\dot{\psi}^2 - V(\phi, \psi) \right) + 8H\dot{\phi}}{\left(-\frac{\omega}{2}\dot{\phi}^2 - \frac{\beta}{2}\dot{\psi}^2 + V(\phi, \psi) \right)}. \quad (22)$$

In the limit $\dot{\phi} \rightarrow 0$, we find

$$w_{eff}|_{\dot{\phi} \rightarrow 0} \simeq \frac{-\frac{\beta}{2}\dot{\psi}^2 - V(\phi_0, \psi)}{-\frac{\beta}{2}\dot{\psi}^2 + V(\phi_0, \psi)}, \quad (23)$$

which means that a quintessence scalar describes the effective fluid field ($\beta < 0$) or a phantom scalar field ($\beta > 0$).

On the other hand, in the limit $\dot{\phi}^2 \rightarrow 0$ and $\dot{\psi}^2 \rightarrow 0$, we derive

$$w_{eff}|_{(\dot{\phi}^2, \dot{\psi}^2) \rightarrow 0} \simeq -1 + \frac{8H\dot{\phi}}{V(\phi, \psi)}, \quad (24)$$

thus, the effective fluid can deviate from the cosmological constant and, for $\frac{8H\dot{\phi}}{V(\phi, \psi)} < 0$, w_{eff} can cross the phantom divide line.

Recently, in [78], the integrability properties of the latter dynamical system were studied using the Noether symmetry approach. Specifically, the potential function $V(\phi, \psi)$ has been constrained by the requirement for the field equations to admit Noether symmetries. As a result, conservation laws. New exact and analytic solutions were determined. However,

in this work, we perform a detailed analysis of the phase space for the dynamical system (14)-(17). Hence, from such analysis, we can reconstruct the cosmological history provided by the multiscalar-torsion model and study the stability properties of the exact solutions determined in [78].

3. FIELD EQUATIONS IN DIMENSIONLESS VARIABLES

We proceed by assuming the scalar field potential to be $V(\phi, \psi)$ to be separable, that is $V(\phi, \psi) = V_1(\phi) + V_2(\psi)$. Consequently, $\hat{V}(\phi, \psi) = -V_2(\psi)F(\phi) - F(\phi)(U(\phi) + V_1(\phi))$, which means that there exist interaction between the two scalar fields as long as $V_2(\psi)$ is a nonconstant function.

In the context of the H -normalization [86] we define the dimensionless variables

$$x = \frac{\dot{\phi}}{\sqrt{12}H}, \quad y = \sqrt{\frac{V_1(\phi)}{6H^2}}, \quad z = \frac{\dot{\psi}}{\sqrt{12}H}, \quad v = \sqrt{\frac{V_2(\psi)}{6H^2}}, \quad (25)$$

$$\lambda = (\ln V_1(\phi))_{,\phi}, \quad \mu = (\ln V_2(\psi))_{,\psi}, \quad \tau = \ln a. \quad (26)$$

In the new variables, the field equations (14)-(17) are written in the equivalent form of an algebraic-differential system of first-order differential equations.

The new dimensionless variables satisfy the following system

$$2\omega \frac{dx}{d\tau} = v^2 (4\sqrt{3} - 3\omega x) + (4\sqrt{3} - 3\omega x) (\omega x^2 + y^2 + \beta z^2 + 1) + 2\sqrt{3}\lambda y^2, \quad (27)$$

$$\frac{dy}{d\tau} = -\frac{1}{2}y (3v^2 - 2\sqrt{3}(\lambda + 4)x + 3\omega x^2 + 3(y^2 + \beta z^2 - 1)), \quad (28)$$

$$2\beta \frac{dz}{d\tau} = v^2 (2\sqrt{3}\mu - 3\beta z) - 3\beta z (\omega x^2 + y^2 + \beta z^2 + 1), \quad (29)$$

$$\frac{dv}{d\tau} = -\frac{1}{2}v (3v^2 + 3\omega x^2 - 8\sqrt{3}x + 3y^2 + 3\beta z^2 - 2\sqrt{3}\mu z - 3), \quad (30)$$

$$\frac{d\lambda}{d\tau} = 2\sqrt{3}x\lambda^2 (\Gamma_1(\lambda) - 1), \quad (31)$$

$$\frac{d\mu}{d\tau} = 2\sqrt{3}z\mu^2 (\Gamma_2(\mu) - 1), \quad (32)$$

with algebraic constraint

$$1 + \omega x^2 + \beta z^2 - y^2 - v^2 = 0. \quad (33)$$

Functions $\Gamma_1(\lambda)$ and $\Gamma_2(\mu)$ are defined as

$$\Gamma_1(\lambda) = \frac{V_{1,\phi\phi}V_1}{(V_{1,\phi})^2} \quad \text{and} \quad \Gamma_2(\mu) = \frac{V_{2,\psi\psi}V_2}{(V_{2,\psi})^2}. \quad (34)$$

With the constraint equation (33), the dimension of the dynamical system is reduced to five. However, for exponential potential $V_1(\phi) = V_{10}e^{\lambda\phi}$ and $V_2(\psi) = V_{20}e^{\mu\psi}$, we obtain constant values λ and μ .

In the following from (32) we derive $v = \sqrt{1 + \omega x^2 + \beta z^2 - y^2}$.

Thus, the dimension of the dynamical system is reduced to three:

$$\frac{dx}{d\tau} = \frac{\sqrt{3}(\lambda y^2 + 4\beta z^2 + 4)}{\omega} - x(3\omega x^2 - 4\sqrt{3}x + 3\beta z^2 + 3), \quad (35)$$

$$\frac{dy}{d\tau} = y(\sqrt{3}(\lambda + 4)x - 3\omega x^2 - 3\beta z^2), \quad (36)$$

$$\frac{dz}{d\tau} = \frac{\sqrt{3}\mu(\omega x^2 - y^2 + \beta z^2 + 1)}{\beta} - 3z(\omega x^2 + \beta z^2 + 1). \quad (37)$$

We proceed with the investigation of the equilibrium points for the three-dimensional dynamical system (35), (36) and (37). Every equilibrium point describes an asymptotic exact cosmological solution with an effective equation of state parameter

$$w_{eff}(x, y, z; \omega, \beta) = -1 - 2(\omega x^2 + \beta z^2) + \frac{8}{\sqrt{3}}x. \quad (38)$$

The deceleration parameter is given by

$$q(x, z; \omega, \beta) = -1 - 3\omega x^2 + 4\sqrt{3}x - 3\beta z^2. \quad (39)$$

For $w_{eff} \neq -1$, the asymptotic solutions have a power-law scale factor $a(t) = a_0 t^{\frac{2}{3(1+w_{eff})}}$, while for $w_{eff} = -1$, the universe is described by the de Sitter solution with $a(t) = a_0 e^{H_0 t}$. For the equilibrium points, we study their stability properties to construct the cosmological history. An equilibrium point characterized as an attractor indicates that the asymptotic solution is stable, while source and saddle points provide unstable solutions. Because the exact cosmological solutions derived before [78] are related to the asymptotic solutions at the equilibrium points. From such analysis, we extract information related to the stability properties of the solutions derived in [78].

By definition, it follows that y and v are positively defined, that is, $y \geq 0$, $v \geq 0$, while for $\omega < 0$ and $\beta = -1$ from the algebraic equation (33), it follows that $|\omega x^2| \leq 1$, $|\beta z^2| \leq 1$, $0 \leq y \leq 1$ and $0 \leq v \leq 1$. Otherwise, for other values of the free parameters ω , β parameters $\{x, y, z, v\}$ are not constrained in the finite regime and can take values at the infinity regime.

4. DYNAMICAL ANALYSIS AT THE FINITE REGIME

The equilibrium points $P = (x(P), y(P), z(P))$ of the field equations (35), (36) and (37) at the finite regime are:

$$P_1^\pm = \left(x_1, 0, \pm \sqrt{-\frac{1 + \omega x_1^2}{\beta}} \right),$$

with $v(P_1^\pm) = 0$, and $w_{eff}(P_1^\pm) = 1 + \frac{8}{\sqrt{3}}x_1$. Because $y(P_1^\pm) = 0$, $v(P_1^\pm) = 0$ we infer that $\lambda\phi(P_1^\pm) \rightarrow -\infty$ and $\mu\psi(P_1^\pm) \rightarrow -\infty$. P_1^\pm are two sets of equilibrium points that exist for $\beta < 0$ and $x_1 = 0$ or $\beta < 0$ and $\frac{1}{x_1^2} + \omega \geq 0$ or $\beta > 0$ and $\frac{1}{x_1^2} + \omega \leq 0$. As a particular case, we use $\beta = \pm 1$, to simplify calculations. The asymptotic solutions at P_1^\pm describe accelerated universes for $x_1 < -\frac{\sqrt{3}}{6}$. The eigenvalues of the linearized system are derived $e_1(P_1^\pm) = 0$, $e_2(P_1^\pm) = 3 + \sqrt{3}(4 + \lambda)x_1$ and $e_3(P_1^\pm) = 6 + 8\sqrt{3}x_1 \pm 2\sqrt{3}\mu\sqrt{-\frac{1 + \omega x_1^2}{\beta}}$. Note that the eigenvector associated with $e_1(P_1^\pm) = 0$ is $\left(\frac{\sqrt{\beta(-\omega x_1^2 - 1)}}{x_1\omega}, 0, 1 \right)$ is proportional to the normal vector to the sets given by $\left(1, 0, \frac{x_1\omega}{\sqrt{\beta(-\omega x_1^2 - 1)}} \right)$ this means that the sets are normally hyperbolic. Their stability is determined by the nonzero eigenvalues $e_2(P_1^\pm), e_3(P_1^\pm)$. To understand the stability properties of points P_1^\pm in Fig. 1, we plot the two-dimensional phase-space portraits for the dynamical system on the surface with $y = 0$. From the phase-space portraits, we remark that points P_1^\pm define surfaces where the trajectories move from infinity to the finite regimes and vice versa.

$$P_2 = \left(\frac{4 + \lambda}{\sqrt{3}\omega}, \sqrt{\frac{(4 + \lambda)^2 + 3\omega}{3\omega}}, 0 \right),$$

with $v(P_2) = 0$, and $w_{eff}(P_2) = -1 - \frac{2\lambda(4 + \lambda)}{\omega}$.

Fig. 2 shows the region of existence of point P_2 where $v(P_2) = 0$.

For this point, only the potential of the second scalar field is zero, from where we infer that $\mu\psi(P_2) \rightarrow -\infty$. The point is real when $\frac{(4 + \lambda)^2 + 3\omega}{3\omega} > 0$. For $\beta = -1$ and $\omega < 0$, it follows that the point is physically accepted for $-\frac{|\omega|}{\sqrt{3}} < 4 + \lambda < \frac{|\omega|}{\sqrt{3}}$. The eigenvalues are derived $e_1(P_2) = -3 - \frac{(4 + \lambda)^2}{\omega}$, $e_2(P_2) = -3 - \frac{(4 + \lambda)^2}{\omega}$ and $e_3(P_2) = -\frac{2\lambda(4 + \lambda)}{\omega}$. Hence, for $\beta = -1$, $\omega < 0$ point P_2 is an attractor when $\left\{ 0 \leq 4 + \lambda \leq \sqrt{3}|\omega|, -\frac{16}{3} < \omega \leq -1 \right\}$ or $\left\{ -4 \leq \lambda \leq 0, \omega \leq -\frac{16}{3} \right\}$ or $\left\{ 0 \leq 4 + \lambda \leq \sqrt{3}|\omega| \right\}$. For other values of β and ω , point P_2 describes a stable solution when $\lambda = -4$ and for a nonzero parameter ω ; or $\lambda = 0$ and

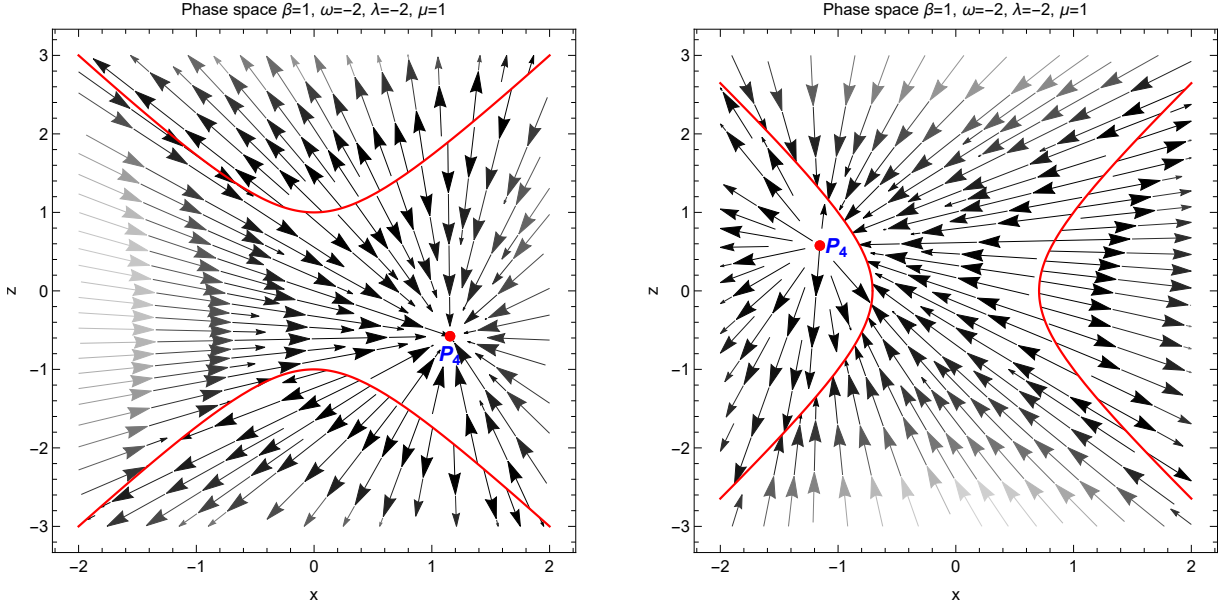


FIG. 1: Two-dimensional phase-space portrait of the dynamical system on the surface $y = 0$. The left plot is for $\beta = 1$ and $\omega = -2$, while the right plot is for $\beta = -1$ and $\omega = 2$. With red lines are the family of points P_1^\pm . From the phase-space portrait, points P_1^\pm define surfaces where the trajectories can move from the finite to the infinity regimes and vice versa.

$\omega \leq -\frac{16}{3}$, or $\omega > 0$, $-4 < \lambda < 0$ and $(4 + \lambda)^2 \leq -3\omega$ and $\omega > 0$ with $\{\lambda < -4, \lambda > 0\}$. In Fig. 3 we give the region of the space of the free parameters λ and ω where point P_2 is an attractor.

Fig. 4 displays a region for the free parameters λ and ω where point P_2 describes an accelerated solution.

In Fig. 5, the evolution of w_{eff} and q is presented. The parameters are evaluated at a numerical solution of (35), (36) and (37) with initial conditions near P_2 , i.e. $x(0) = \frac{\lambda+4}{\sqrt{3\omega}} + 0.1, y(0) = \frac{\sqrt{(\lambda+4)^2+3\omega}}{\sqrt{3\omega}} + 0.1, z(0) = 0.1$. This figure shows that for early time $w_{eff} > -\frac{1}{3}$ and $q > 0$; therefore, there is an early-time deceleration phase. Later evolution enters a matter-dominated phase when $w_{eff} = 0$ and $q = \frac{1}{2}$. Quickly after that, we see that the behaviour describes late time acceleration for $w_{eff} < -\frac{1}{3}$ and $q < 0$. We also see a transient de Sitter behaviour since both cross the value $w_{eff} = q = -1$. Finally, they cross to the phantom regime $w_{eff} < -1$ and $q < -1$ with a transient damped oscillation in both parameters. The evolution of the x, y and z variables in the time τ are presented for completeness.

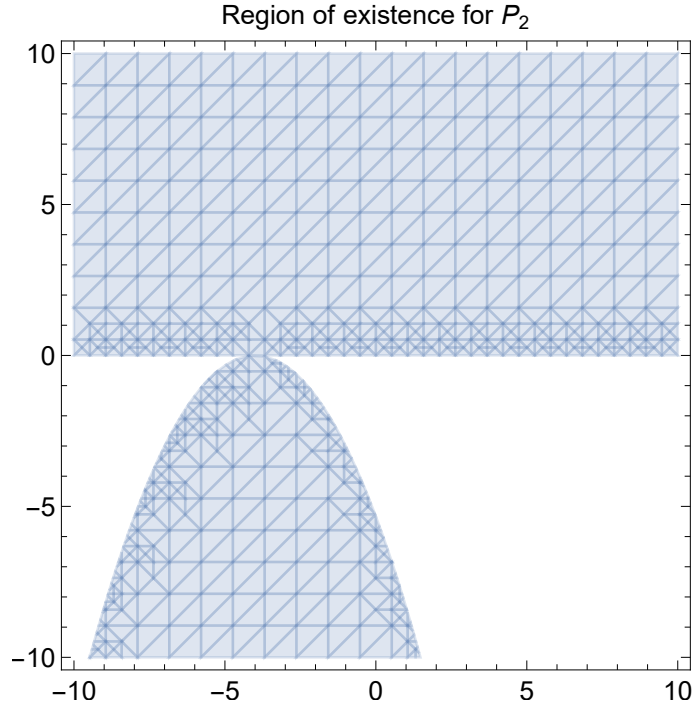


FIG. 2: Region of existence of point P_2 where $v(P_2) = 0$.

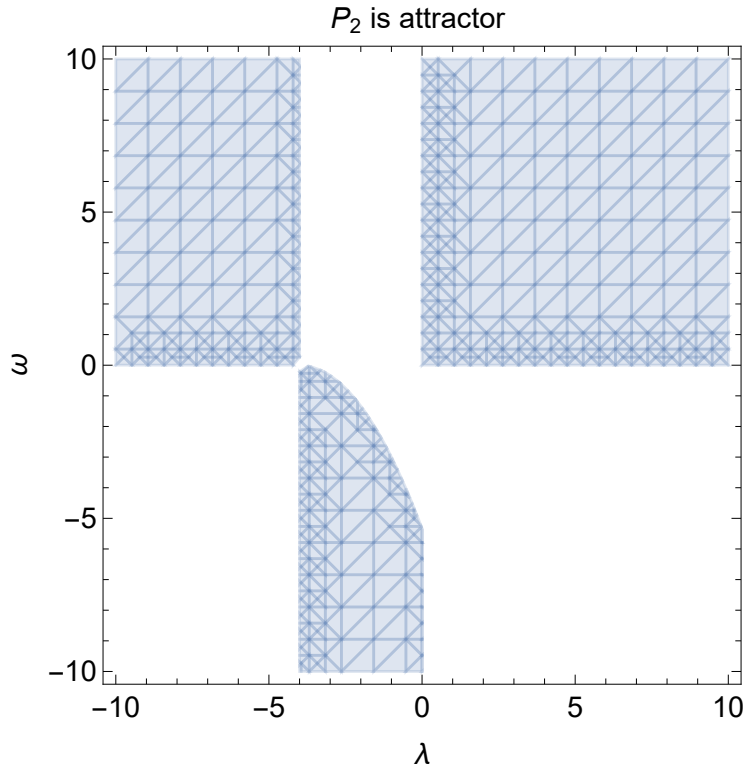


FIG. 3: Region plot on the space of the free parameters λ and ω where point P_2 is an attractor.

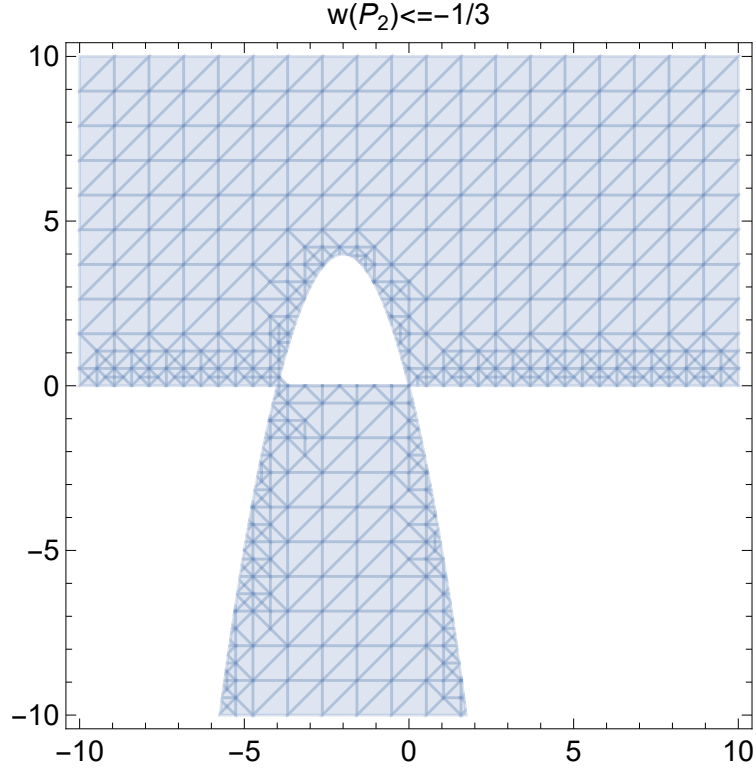


FIG. 4: Region for the free parameters λ and ω where point P_2 describes an accelerated solution.

$$P_3 = \left(\frac{(4 + \lambda) \mu^2}{\sqrt{3} (\beta \lambda^2 + \omega \mu^2)}, \sqrt{-\frac{(4\beta\lambda - \omega\mu^2) (3(\beta\lambda^2 + \omega\mu^2) + \mu^2(4 + \lambda)^2)}{3(\beta\lambda^2 + \omega\mu^2)^2}}, \frac{(4 + \lambda) \lambda \mu}{\sqrt{3} (\beta \lambda^2 + \omega \mu^2)} \right),$$

with $v(P_3) = \sqrt{\frac{\beta\lambda(4+\lambda)(3\beta\lambda^2+\mu^2((4+\lambda)^2+3\omega))}{3(\beta\lambda^2+\omega\mu^2)^2}}$, and $w_{eff}(P_3) = -1 - \frac{2\lambda(4+\lambda)\mu^2}{3(\beta\lambda^2+\omega\mu^2)}$. Therefore $\phi(P_3)$ and $\psi(P_4)$ are defined in the finite regime. In Fig. 6, we present the region in the space of the free parameters λ and ω where the point is real and physically accepted. Because of the nonlinear form of the eigenvalues, the stability properties are investigated numerically. In Fig. 7 we present the region in the space of the free parameters λ and ω where the equilibrium point P_3 is an attractor for $\mu = 1$. Moreover, in Fig. 8 we present the values of the free parameters λ and ω where the asymptotic solution at point P_3 describes an accelerated universe, i.e. $w(P_3) < -\frac{1}{3}$.

$$P_4 = \left(\frac{4\sqrt{3}}{3\omega}, 0, \frac{\sqrt{3}\mu}{3\beta} \right),$$

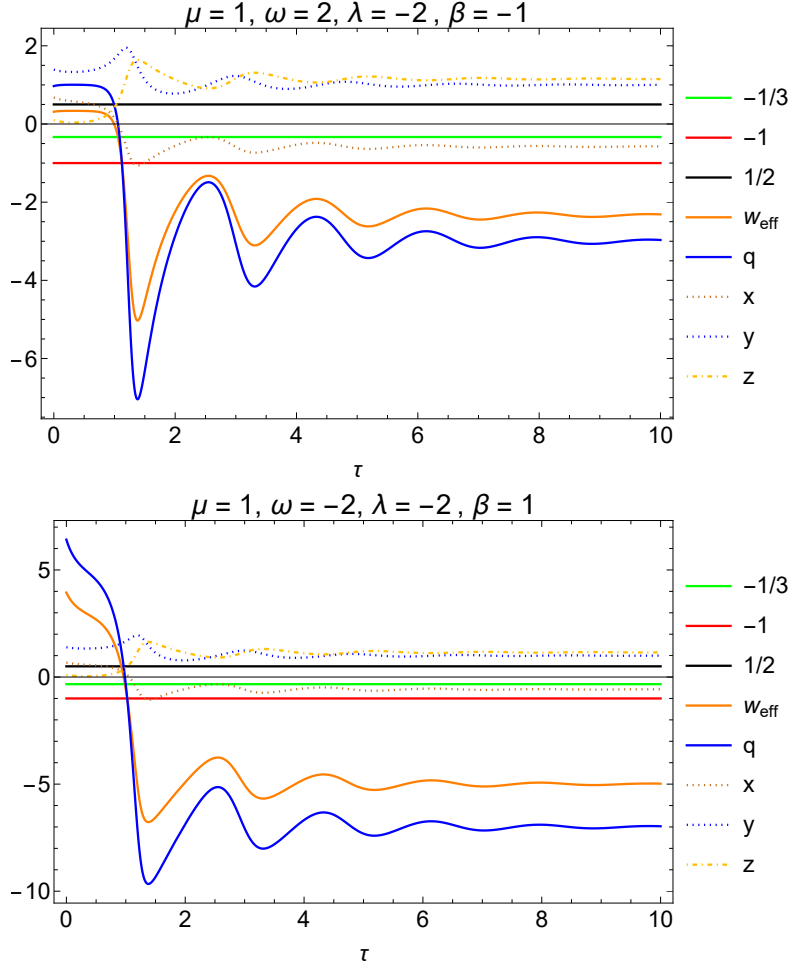


FIG. 5: Evolution of w_{eff} and q evaluated at a numerical solution of system (35), (36) and (37) with initial conditions near P_2 , i.e. $x(0) = \frac{\lambda+4}{\sqrt{3}\omega} + 0.1, y(0) = \frac{\sqrt{(\lambda+4)^2+3\omega}}{\sqrt{3}\sqrt{\omega}} + 0.1, z(0) = 0.1$ for different values of the parameters $\mu, \beta, \omega, \lambda$. We see that for early time $w_{eff} > -\frac{1}{3}$ and $q > 0$, meaning there is an early-time deceleration phase. Later, it enters a matter-dominated phase when $w_{eff} = 0$ and $q = \frac{1}{2}$ but quickly after that, we see that the behaviour describes late time acceleration for $w_{eff} < -\frac{1}{3}$ and $q < 0$. We also see a transient de Sitter behaviour since both cross the value $w_{eff} = q = -1$. Finally, they cross to the phantom regime $w_{eff} < -1$ and $q < -1$ with a transient damped oscillation in both parameters.

with $v(P_4) = \sqrt{1 + \frac{1}{3} \left(\frac{\mu^2}{\beta} + \frac{16}{\omega} \right)}$, and $w_{eff}(P_4) = -1 - \frac{3\mu^2}{2\beta}$. Hence, $\lambda\phi(P_4) \rightarrow -\infty$, and $\psi(P_4)$ is defined in the finite regime. The point is real and physically accepted for the regions shown in Fig. 9. Some particular cases of interest are the following: for $-\frac{3}{16} - \frac{\mu^2}{16\beta} < \frac{1}{\omega}$; on the other hand for $\omega < 0$ and $\beta = -1$, P_4 is physically accepted for $\mu^2 < 3, (\mu^2 - 3)\omega \geq 16$.

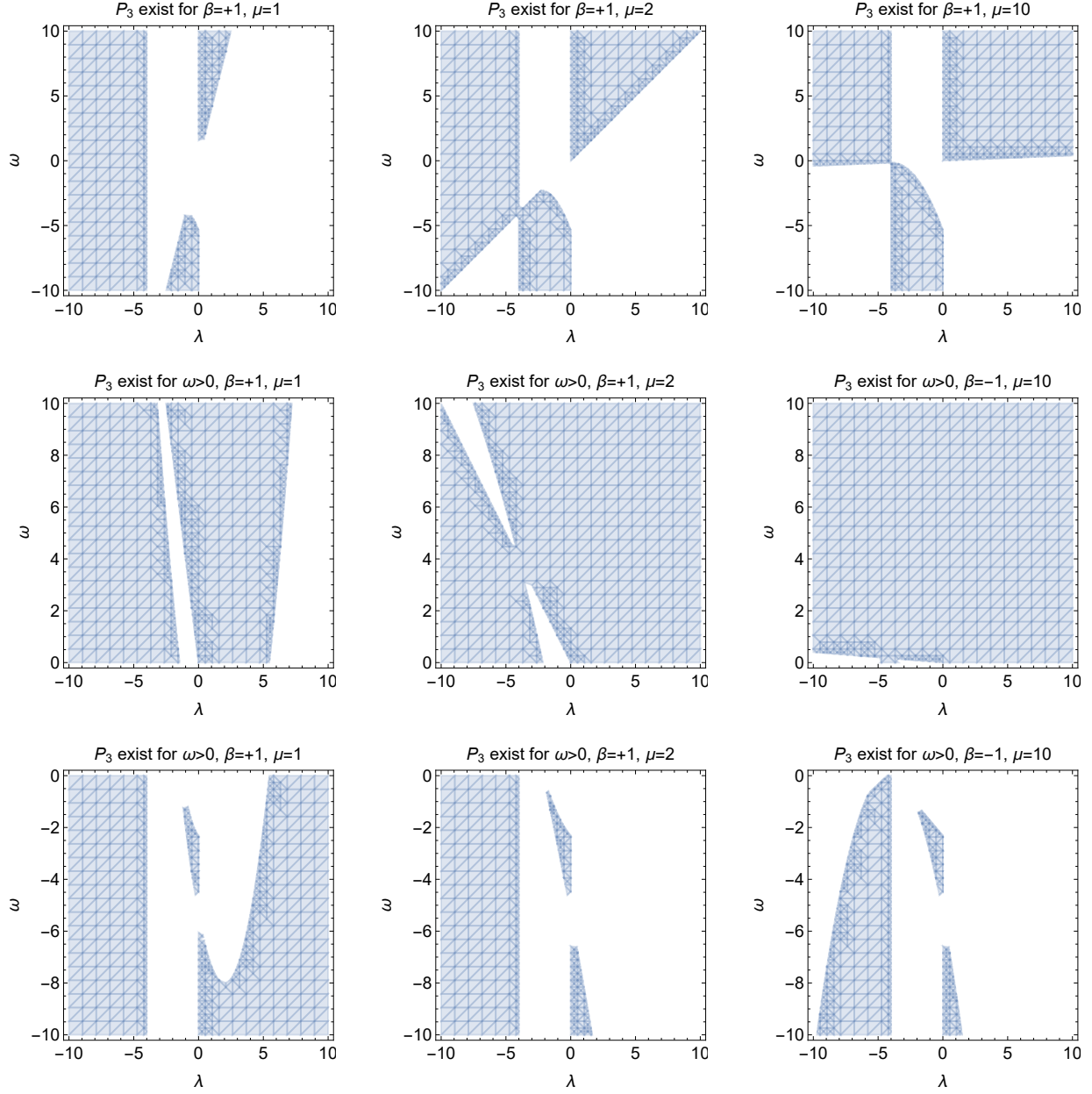


FIG. 6: Region plot on the space of the free parameters λ and ω for different values of μ where point P_3 exists. The figures in the first row are for $\beta = +1$; while figures of the second row and the third row are for $\beta = -1$.

For $\beta = -1$, the asymptotic solution describes an accelerated universe for $|\mu| < \frac{2}{3}$, while for $\beta = +1$, the asymptotic solution always describes acceleration with $w_{eff}(P_4)|_{\beta=1} < -1$. The eigenvalues of the linearized system near the stationary point are $e_1(P_4) = -\frac{\mu^2}{\beta} + \frac{4\lambda}{\omega}$, $e_2(P_4) = -3 - \frac{\mu^2}{\beta} - \frac{16}{\omega}$ and $e_3(P_4) = e_2(P_4)$.

Consequently, the equilibrium point P_4 is an attractor for $\mu = 0$ with $\{\lambda < 0, \omega > 0\}$ or

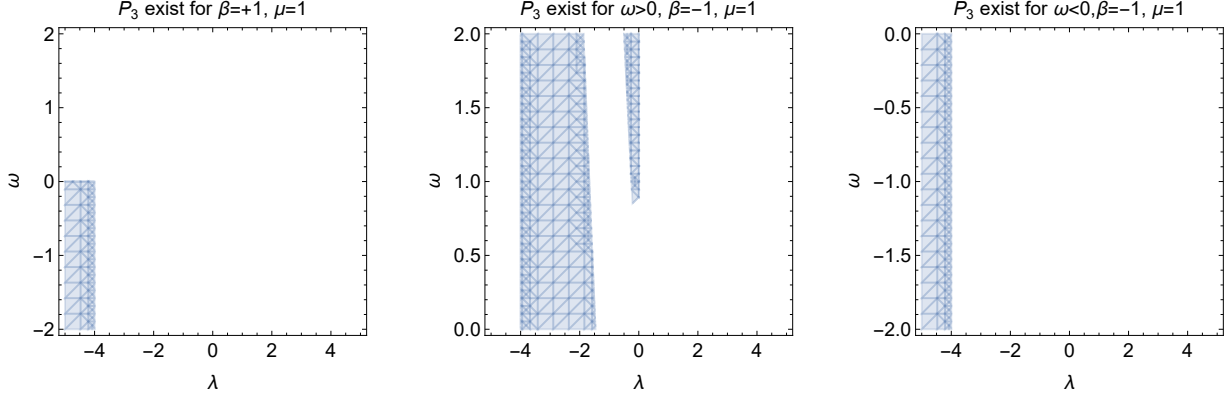


FIG. 7: Region plot on the space of the free parameters λ and ω for μ where point P_3 is an attractor.

TABLE I: Equilibrium points for the multi-torsion cosmological model (35), (36) and (37) in the finite regime.

Points	w_{eff}	q	Acceleration?	Attractor?
P_1^\pm	$1 + \frac{8}{\sqrt{3}}x_1$	$4\sqrt{3}x_1 + 2$	$x_1 < -\frac{\sqrt{3}}{6}$	No
P_2	$-1 - \frac{2\lambda(4+\lambda)}{\omega}$	$-\frac{\lambda(\lambda+4)+\omega}{\omega}$	Yes (Fig. 4)	Yes (Fig. 3)
P_3	$-1 - \frac{2\lambda(4+\lambda)\mu^2}{3(\beta\lambda^2+\omega\mu^2)}$	$-\frac{\beta\lambda^2+\mu^2(\lambda(\lambda+4)+\omega)}{\beta\lambda^2+\mu^2\omega}$	Yes (Fig. 8)	Yes (Fig. 7)
P_4	$-1 - \frac{2\mu^3}{2\beta}$	$-\frac{\beta+\mu^2}{\beta}$	$\beta + \mu^2 < 0$ or $\beta > 0$	Yes (Fig. 10)

$\{\lambda > 0, \omega < -\frac{16}{3}\}$ for arbitrary β . In the case where $\beta = +1$, point P_4 is an attractor for $\{\lambda < -\frac{4\mu^2}{3+\mu^2}, 0 < \omega < \frac{4\lambda}{\mu^2}\}$, or $\{-\frac{4\mu^2}{3+\mu^2} < \lambda < 0, 0 < \omega\}$, or $\{-\frac{4\mu^2}{3+\mu^2} < \lambda < 0, \omega < -\frac{16}{3+\mu^2}\}$ or $\{\lambda > 0, \omega < -\frac{16}{3+\mu^2}\}$ or $\{\lambda > 0, \frac{4\lambda}{\mu^2} < \omega\}$.

On the other hand, for $\beta = -1$, point P_4 is an attractor for $\mu^2 < 3$ with $\{\lambda < 0, \omega > 0, \omega < -\frac{4\lambda}{\mu}\}$ or $\{\omega > -\frac{4\lambda}{\mu^2}, \frac{\mu^2(4+\lambda)}{3} < \lambda, \omega < \frac{16}{\mu^2-3}\}$, or $\mu > 3$ with $\{\lambda \leq -\frac{4\mu^2}{\mu^2-3}, 0 < \omega < \frac{16}{\mu^2-3}\}$ or $\{-\frac{4\mu^2}{\mu^2-3} < \lambda < 0, 0 < \omega < -\frac{4\lambda}{\mu}\}$ and for $\mu = 3$, $\{0 < \omega < -\frac{4\lambda}{3}, \lambda > 0\}$.

Last but not least, for $\omega < 0, \beta = -1$ the equilibrium point is an attractor when $\mu^2 < 3, (\mu^2 - 3)\omega \geq 16$ and $4\lambda + \mu\omega > 0$. In Fig. 10 we present the graphic illustration of the latter regions.

In Table I, we summarize the results of the dynamical analysis at the finite regime.

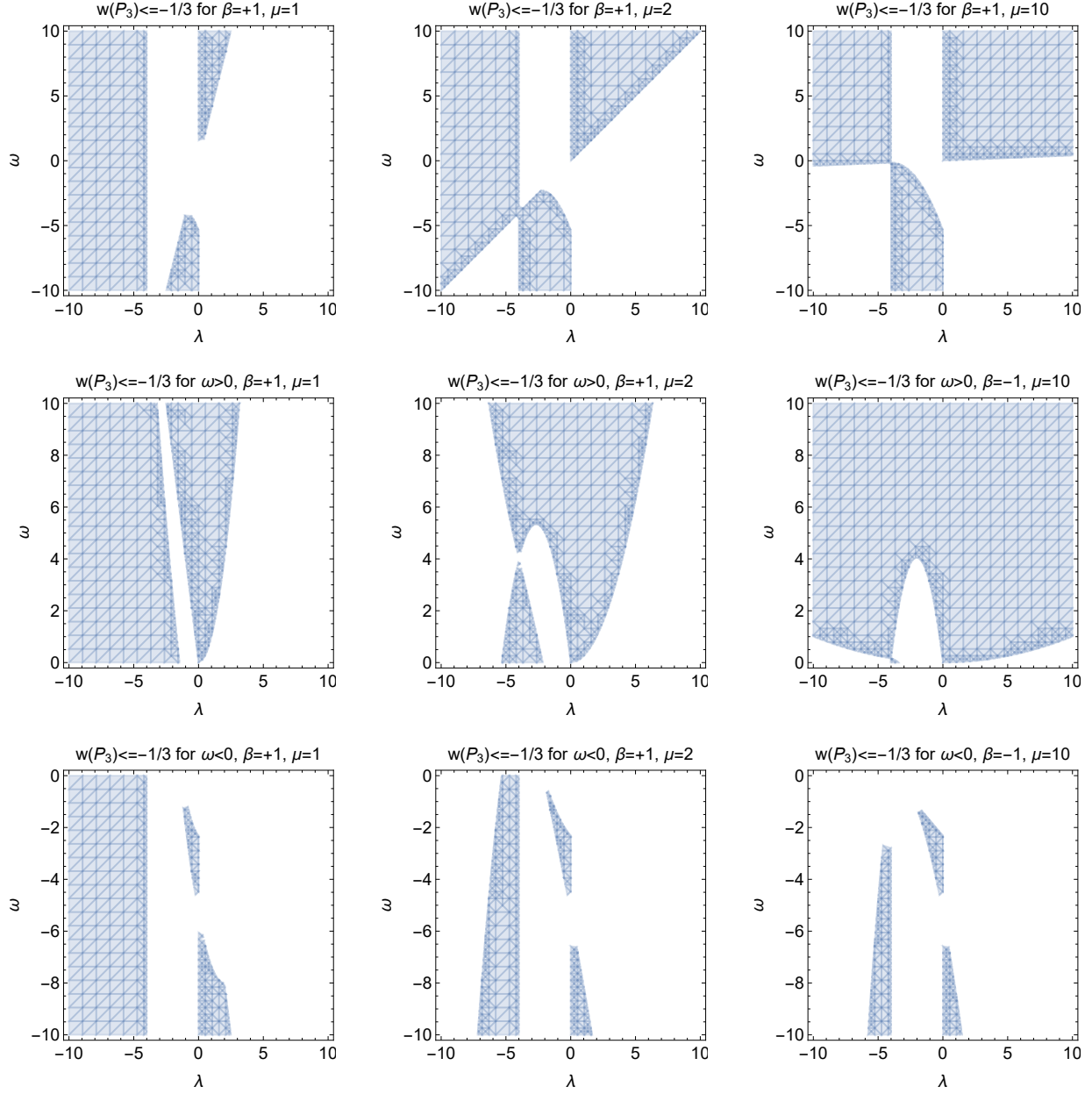


FIG. 8: Region plot on the space of the free parameters λ and ω for different values of μ where $w(P_3) < -\frac{1}{3}$. Figures of the first row are for $\beta = +1$, while figures of the second row and the third row are for $\beta = -1$.

To finish this section, in Fig. 11 is shown a three-dimensional phase-space portrait of the full system (35), (36) and (37). The values $\lambda = -2, \mu = 1, \beta = -1, \omega = 2$ were considered in the left plot. The values $\lambda = -2, \mu = 1, \beta = 1, \omega = -2$ were considered in the right plot. The planes that contain the hyperbolas in both portraits are the $y = 0$ projections shown in Fig. 1.

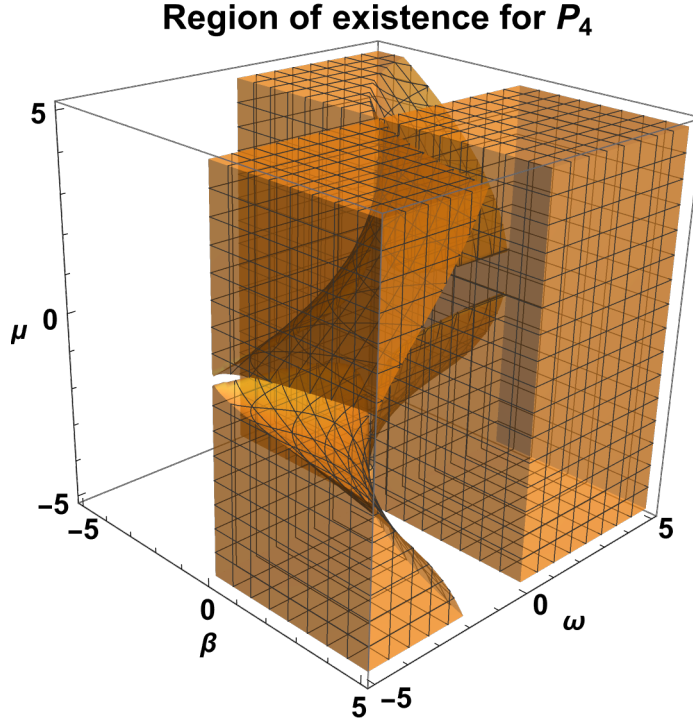


FIG. 9: Region of existence of point P_4 where $v(P_4) \geq 0$, that is $\frac{\mu^2}{3\beta} + \frac{16}{3\omega} + 1 \geq 0$.

5. DYNAMICAL ANALYSIS AT THE INFINITY REGIME

Owing to the fact that the dynamical system (35), (36) and (37) is non-compact, there could be features in the asymptotic regime which are non-trivial for the global dynamics. Thus, we will extend our study using the Poincaré method to complete the phase space analysis. We define the Poincaré variables

$$x = \frac{\rho}{\sqrt{1-\rho^2}} \sin \theta_1 \cos \theta_2, \quad y = \frac{\rho}{\sqrt{1-\rho^2}} \sin \theta_1 \sin \theta_2, \quad z = \frac{\rho}{\sqrt{1-\rho^2}} \cos \theta_1.$$

The inverse transformation is

$$\rho = \frac{\sqrt{x^2 + y^2 + z^2}}{\sqrt{x^2 + y^2 + z^2 + 1}}, \quad \theta_1 = \tan^{-1} \left(\frac{\sqrt{x^2 + y^2}}{z} \right), \quad \theta_2 = \tan^{-1} \left(\frac{y}{x} \right).$$

We have chosen these spherical coordinates where θ_1 is the azimuth angle measured with respect to the z -axis. Because y is non-negative by definition, and x and z can have either sign (θ_2 is the polar angle) the physical region is $0 \leq \rho \leq 1$, $\theta_1 \in [0, \pi]$ and $\theta_2 \in [0, \pi]$. Infinity is reached when $\rho \rightarrow 1$.

We consider the new independent variable $\frac{d}{dT} = \sqrt{1-\rho^2} \frac{d}{dt}$, thus the dynamical system (27)-(28) with the use of the constraint equation (33) is expressed in terms of the variables

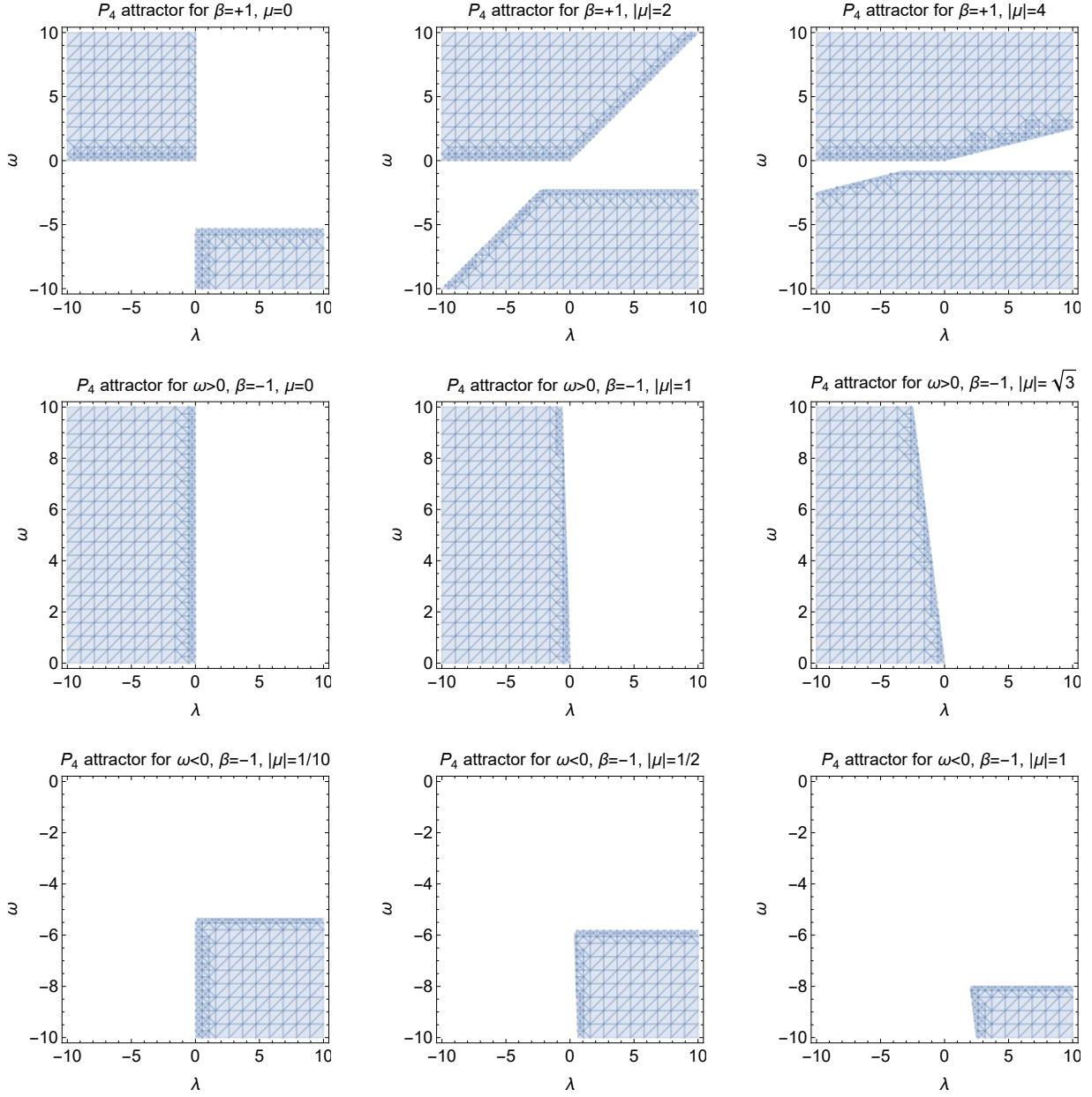


FIG. 10: Region plot on the space of the free parameters λ and ω for different values of μ^2 where point P_4 is an attractor. The figures in the first row are for $\beta = +1$; while figures of the second row are for $\beta = -1$.

$\{T, \rho, \theta_1, \theta_2\}$ in the following form

$$\frac{d\rho}{dT} = f_1(\rho, \theta_1, \theta_2), \quad (40)$$

$$\frac{d\theta_1}{dT} = f_2(\rho, \theta_1, \theta_2), \quad (41)$$

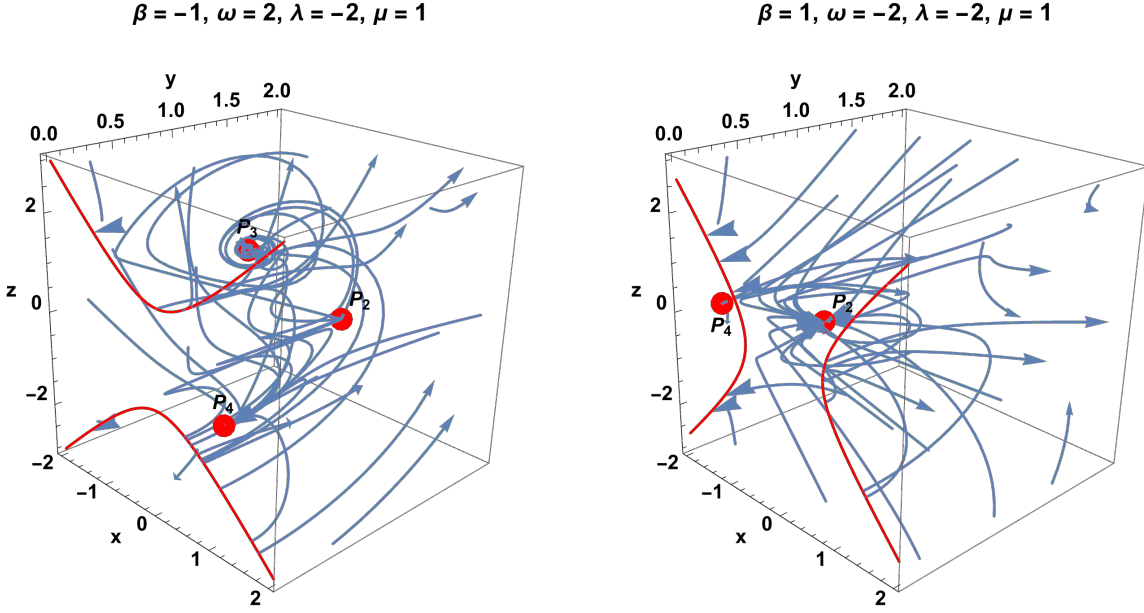


FIG. 11: Three-dimensional phase-space portrait of the full system (35), (36) and (37). In the left plot, the values $\lambda = -2, \mu = 1, \beta = -1, \omega = 2$ were considered. In the right plot, the values $\lambda = -2, \mu = 1, \beta = 1, \omega = -2$ were considered. The planes that contain the hyperbolas in both portraits are the $y = 0$ projections shown in Fig. 1

$$\frac{d\theta_2}{dT} = f_3(\rho, \theta_1, \theta_2), \quad (42)$$

where f_1 , f_2 and f_3 are nonlinear expressions. At the finite regime, $\rho \rightarrow 1$, the leading terms of the latter dynamical system reads

$$\frac{1}{\sqrt{1-\rho}} \frac{d\rho}{dT} = -\frac{3}{4} \left((2\beta - \omega) \cos(2\theta_1) + 2\beta + 2\omega \sin^2(\theta_1) \cos(2\theta_2) + \omega \right), \quad (43)$$

$$\begin{aligned} \frac{d\theta_1}{dT} = \frac{\sqrt{3}}{8\beta\omega} & \left[\beta \cos(\theta_1) \left(\cos(\theta_2) (\cos(2\theta_1) (16\beta - \lambda(\omega + 1) - 16\omega) + 16\beta + \lambda\omega + \lambda + 16\omega) \right. \right. \\ & \left. \left. - 2\lambda(\omega + 1) \sin^2(\theta_1) \cos(3\theta_2) \right) \right. \\ & \left. - \mu\omega \left((2\beta + 3\omega - 3) \sin(\theta_1) + (2\beta - \omega + 1) \sin(3\theta_1) + 4(\omega + 1) \sin^3(\theta_1) \cos(2\theta_2) \right) \right], \quad (44) \end{aligned}$$

$$\frac{d\theta_2}{dT} = \frac{\sqrt{3} \sin(\theta_1) \sin(\theta_2) (-4\beta \cot^2(\theta_1) + \lambda\omega \cos^2(\theta_2) - \lambda \sin^2(\theta_2))}{\omega}. \quad (45)$$

We represent the infinite regime in the right hemisphere of the Poincaré sphere,

$$X = \rho \sin \theta_1 \cos \theta_2, \quad Y = \rho \sin \theta_1 \sin \theta_2, \quad Z = \rho \cos \theta_1.$$

The radial equations do not contain the radial coordinate, so the equilibrium points can only be obtained using the angular equations. Setting $\frac{d\theta_1}{dT} = 0, \frac{d\theta_2}{dT} = 0$, we obtain the equilibrium points listed in table II. These points' stability is studied by first analyzing the angular coordinates' stability and then deducing the stability in the radial direction from the equation (43). In these variables, infinity is reached when $\rho \rightarrow 1$. Hence, a point at infinity is stable in the radial direction when $\frac{d\rho(T)}{dT} > 0$, which means that $\rho(T)$ is a monotonic increasing function that tends towards $\rho = 1$ from below. When $\frac{d\theta_1}{dT} < 0$, the equilibrium points at infinity are either saddles or sources, depending on the radial stability. When $\frac{d\rho(T)}{dT} = 0$, the method is not conclusive, so we resort to numerical inspection.

In the following analysis, the eigenvalue $e_1(Q)$ corresponds to the radial direction the equation (43) gives. Consequently, the equilibrium points $Q := (X, Y, Z)$ at the infinite regime are $Q_1^+ = \left(\frac{1}{\sqrt{\omega+1}}, \sqrt{\frac{\omega}{\omega+1}}, 0\right)$, and $Q_2^+ = \left(-\frac{1}{\sqrt{\omega+1}}, \sqrt{\frac{\omega}{\omega+1}}, 0\right)$, they exist for $\omega \geq 0$.

The eigenvalues are $e_1(Q_1^+) = e_1(Q_2^+) = -\frac{3\omega}{\omega+1}$, $e_2(Q_1^+) = -\frac{2\sqrt{3}\lambda}{\sqrt{\omega+1}} = -e_2(Q_2^+)$, $e_3(Q_1^+) = -\frac{\sqrt{3}(\lambda+4)}{\sqrt{\omega+1}} = -e_3(Q_2^+)$. This means that Q_1^+ is source for $\{\omega > 0, \lambda < -4\}$ and a saddle for $\{-4 < \lambda < 0, \omega > 0\}$.

On the other hand, Q_2^+ is a source for $\{\lambda > 0, \omega > 0\}$ and a saddle for $\{-4 < \lambda < 0, \omega > 0\}$.

The following points are $Q_3^+ = \left(\sqrt{\frac{\beta}{\beta-\omega}}, 0, \sqrt{\frac{\omega}{\omega-\beta}}\right)$, $Q_4^+ = \left(-\sqrt{\frac{\beta}{\beta-\omega}}, 0, -\sqrt{\frac{\omega}{\omega-\beta}}\right)$, $Q_5^+ = \left(\sqrt{\frac{\beta}{\beta-\omega}}, 0, -\sqrt{\frac{\omega}{\omega-\beta}}\right)$, $Q_6^+ = \left(-\sqrt{\frac{\beta}{\beta-\omega}}, 0, \sqrt{\frac{\omega}{\omega-\beta}}\right)$, they all exist for $\omega < 0$ and $\beta \geq 0$ or $\omega > 0$ and $\beta \leq 0$ or $\omega = 0$ and $\beta \neq 0$. Also, the eigenvalue in the radial direction $e_1(Q_i^+) = 0$ for $i = 3, 4, 5, 6$.

As a particular case, we use $\beta = \pm 1$ to simplify calculations.

The eigenvalues for Q_3^+ are $e_2(Q_3^+) = \frac{\sqrt{3}\sqrt{\beta}(\lambda+4)}{\sqrt{\beta-\omega}}$, $e_3(Q_3^+) = \frac{2\sqrt{3}(\mu\sqrt{\omega}+4i\sqrt{\beta})}{\sqrt{\omega-\beta}}$.

In the 2-dimensional projection, Q_3^+ is an attractor for $\{\lambda < -4, \mu < 0, \omega < -\frac{16}{\mu^2}\}$.

Q_3^+ is a source for $\{\omega = 0, \lambda > -4$ or $\lambda > -4, \mu < 0, -\frac{16}{\mu^2} < \omega < 0\}$ or $\{\lambda > -4, \mu \geq 0, \omega < 0\}$ it is also a saddle in any other case.

The eigenvalues for the points Q_4^+ are the opposite of the eigenvalues of Q_3^+ , that is $e_2(Q_4^+) = -\frac{\sqrt{3}\sqrt{\beta}(\lambda+4)}{\sqrt{\beta-\omega}} = -e_2(Q_3^+)$, $e_3(Q_4^+) = \frac{2\sqrt{3}(-\mu\sqrt{\omega}-4i\sqrt{\beta})}{\sqrt{\omega-\beta}} = -e_3(Q_3^+)$. That means that the dynamics of Q_4^+ are reversed.

Similarly, for Q_5^+ and Q_6^+ their respective eigenvalues are opposite, they are $e_2(Q_5^+) = \frac{\sqrt{3}\sqrt{\beta}(\lambda+4)}{\sqrt{\beta-\omega}}$, $e_3(Q_5^+) = \frac{2\sqrt{3}(-\mu\sqrt{\omega}+4i\sqrt{\beta})}{\sqrt{\omega-\beta}}$ and $e_2(Q_6^+) = -\frac{\sqrt{3}\sqrt{\beta}(\lambda+4)}{\sqrt{\beta-\omega}}$, $e_3(Q_6^+) = \frac{2\sqrt{3}(\mu\sqrt{\omega}-4i\sqrt{\beta})}{\sqrt{\omega-\beta}}$,

since the dynamics are reversed, we present the analysis for Q_5^+ .

In the 2-dimensional projection, this point is an attractor for $\{\lambda < -4, \mu > 0, \omega < -\frac{16}{\mu^2}\}$, and a source for $\{\omega = 0, \lambda > -4 \text{ or } \lambda > -4, \mu \leq 0, \omega < 0\}$ or $\{\lambda > -4, \mu > 0, -\frac{16}{\mu^2} < \omega < 0\}$ it is also a saddle in any other case.

The points $Q_7^+ = \left(\frac{4\beta}{\sqrt{16\beta^2 + \mu^2\omega^2}}, 0, \frac{\mu\omega}{\sqrt{16\beta^2 + \mu^2\omega^2}} \right)$, and $Q_8^+ = \left(-\frac{4\beta}{\sqrt{16\beta^2 + \mu^2\omega^2}}, 0, -\frac{\mu\omega}{\sqrt{16\beta^2 + \mu^2\omega^2}} \right)$, both exist for $16\beta^2 + \mu^2\omega^2 > 0$, share the same eigenvalue in the radial direction $e_1(Q_7^+) = e_1(Q_8^+) = -\frac{3\omega(\mu^2\omega+16)}{\mu^2\omega^2+16}$ and also have opposite eigenvalues in the 2-dimensional projection, they are $e_2(Q_7^+) = \frac{\sqrt{3}(4\lambda-\mu^2\omega)}{\sqrt{\mu^2\omega^2+16}} = -e_2(Q_8^+)$, $e_3(Q_7^+) = -\frac{\sqrt{3}(\mu^2\omega+16)}{\sqrt{\mu^2\omega^2+16}} = -e_3(Q_8^+)$.

The point Q_7^+ is an attractor for $\{\beta > 0, \omega < 0, -4\sqrt{-\frac{\beta}{\omega}} < \mu < 4\sqrt{-\frac{\beta}{\omega}}, \lambda < \frac{\mu^2\omega}{4\beta}\}$ or $\{\beta < 0, \omega > 0, \mu < -4\sqrt{-\frac{\beta}{\omega}}, \lambda > \frac{\mu^2\omega}{4\beta}\}$ or $\{\mu > 4\sqrt{-\frac{\beta}{\omega}}, \lambda > \frac{\mu^2\omega}{4\beta}\}$, a source for $\{\beta > 0, \omega < 0, \mu < -4\sqrt{-\frac{\beta}{\omega}}, \lambda > \frac{\mu^2\omega}{4\beta}\}$ or $\{\mu > 4\sqrt{-\frac{\beta}{\omega}}, \lambda > \frac{\mu^2\omega}{4\beta}\}$ or $\{\beta < 0, \omega > 0, -4\sqrt{-\frac{\beta}{\omega}} < \mu < 4\sqrt{-\frac{\beta}{\omega}}, \lambda < \frac{\mu^2\omega}{4\beta}\}$ and a saddle in any other case.

The point Q_8^+ is an attractor for $\{\lambda < 0, \omega < 0, \beta < 0\}$ or $\{\mu \neq 0, \lambda = 0, \omega < 0, \beta < 0\}$ or $\{\mu \neq 0, \lambda > 0, \omega < 0, \frac{\mu^2\omega}{4\lambda} < \beta < 0\}$ a source for $\{\lambda < 0, \omega > 0, \beta > 0\}$ or $\{\mu \neq 0, \lambda = 0, \omega > 0, \beta > 0\}$ or $\{\mu \neq 0, \lambda > 0, \omega > 0, 0 < \beta < \frac{\mu^2\omega}{4\lambda}\}$ and a saddle in any other case.

Finally the points

$$Q_9^+ = \left(\frac{\mu}{\sqrt{-4\beta\lambda + \lambda^2 + \mu^2(\omega + 1)}}, \frac{\sqrt{4\beta\lambda - \mu^2\omega}}{\sqrt{4\beta\lambda - \lambda^2 - \mu^2(\omega + 1)}}, \frac{\lambda}{\sqrt{-4\beta\lambda + \lambda^2 + \mu^2(\omega + 1)}} \right),$$

$$Q_{10}^+ = \left(-\frac{\mu}{\sqrt{-4\beta\lambda + \lambda^2 + \mu^2(\omega + 1)}}, \frac{\sqrt{4\beta\lambda - \mu^2\omega}}{\sqrt{4\beta\lambda - \lambda^2 - \mu^2(\omega + 1)}}, -\frac{\lambda}{\sqrt{-4\beta\lambda + \lambda^2 + \mu^2(\omega + 1)}} \right),$$

They exist for $\lambda < 0, \beta \geq \frac{\mu^2\omega}{4\lambda}$ or $\mu \neq 0, \lambda = 0, \omega \geq 0$ or $\lambda > 0, \beta \leq \frac{\mu^2\omega}{4\lambda}$. The eigenvalue in the radial direction for both points is $e_1(Q_9^+) = e_1(Q_{10}^+) = -\frac{3(\beta\lambda^2 + \mu^2\omega)}{-4\beta\lambda + \lambda^2 + \mu^2(\omega + 1)}$. However the other two eigenvalues are complicated expressions that depend on the four parameters $\lambda, \mu, \omega, \beta$, that is $e_2(Q_9^+) = f_1(\lambda, \mu, \omega, \beta)$, $e_3(Q_9^+) = f_2(\lambda, \mu, \omega, \beta)$ and $e_2(Q_{10}^+) = g_1(\lambda, \mu, \omega, \beta)$, $e_3(Q_{10}^+) = g_2(\lambda, \mu, \omega, \beta)$.

For some values in which these points exist, the real part of the eigenvalues are as follows. For Q_9^+ , with the values $\beta = 1, \omega = -2, \lambda = -2, \mu = 1$ we have $\left\{ -\frac{6}{11}, 4\sqrt{\frac{3}{11}}, -6\sqrt{\frac{3}{11}} \right\}$ which mean saddle behaviour. With the values $\beta = 1, \omega = 2, \lambda = -2, \mu = 1$ we have $\left\{ -\frac{6}{5}, -\frac{1}{\sqrt{5}}, -\frac{1}{\sqrt{5}} \right\}$ this means that it has saddle behaviour (recall, ρ' must be positive for the

stability along the radial direction); For Q_{10}^+ , with the values $\beta = 1, \omega = -2, \lambda = -2, \mu = 1$ we have $\left\{-\frac{6}{11}, -4\sqrt{\frac{3}{11}}, 6\sqrt{\frac{3}{11}}\right\}$ which mean saddle behaviour. With the values $\beta = 1, \omega = 2, \lambda = -2, \mu = 1$ we have $\left\{-\frac{6}{5}, \frac{1}{\sqrt{5}}, \frac{1}{\sqrt{5}}\right\}$ showing source behaviour.

In addition, parameter v should always be real and have a positive value. Thus, for points Q_i^+ we calculate $v(Q_i^+) = 1$ for $i = 1, \dots, 8$, while $v(Q_{9,10}^+) = \sqrt{\frac{\beta\lambda(\lambda+4)}{-4\beta\lambda+\lambda^2+\mu^2(\omega+1)}} + 1$, which means that they exist for $\frac{\beta\lambda(\lambda+4)}{-4\beta\lambda+\lambda^2+\mu^2(\omega+1)} > -1$.

The effective equation of the state parameter and deceleration parameter in the Poincaré variables are expressed as

$$w_{eff}(\rho, \theta_1, \theta_2) = -1 - \frac{2\rho^2}{1-\rho^2} \sin^2 \theta_1 (\omega \cos^2 \theta_2 + \beta \sin^2 \theta_2) + \frac{8}{\sqrt{3}} \frac{\rho}{\sqrt{1-\rho^2}} \sin \theta_1 \cos \theta_2, \quad (46)$$

$$q(\rho, \theta_1, \theta_2) = \frac{1-\rho^2+3\beta\rho^2\cos^2\theta_1}{-1+\rho^2} + \frac{\rho\cos\theta_2\sin\theta_1\left(-4\sqrt{3-3\rho^2}+3\rho\omega\cos\theta_2\sin\theta_1\right)}{-1+\rho^2}. \quad (47)$$

Consequently, these values are expected to be divergent when evaluated in the points Q_i^+ at infinity; in what follows, we show the leading terms of the series centred on $\rho = 1$ to understand the behaviour of the parameters at infinity.

Since Q_1^+ and Q_2^+ exist for $\omega > 0$ we see that $w_{eff}(Q_i^+) \simeq \frac{\omega}{(\rho-1)(\omega+1)}$ and $q(Q_i^+) \simeq \frac{3\omega}{2(\rho-1)(\omega+1)}$ behave as $w_{eff}(Q_i^+) \rightarrow (-\infty)\omega$, $q(Q_i^+) \rightarrow (-\infty)\omega$ for $i = 1, 2$. Therefore, these points describe Big Rip singularities. For points $i = 3, 4, 5, 6$ we have $w_{eff}(Q_i^+) \simeq -\frac{4\sqrt{\frac{2}{3}}\sqrt{\beta}}{\sqrt{1-\rho}\sqrt{\beta-\omega}} - 1$, $q(Q_i^+) \simeq -\frac{2\sqrt{6}\sqrt{\beta}}{\sqrt{1-\rho}\sqrt{\beta-\omega}} - 1$. Clearly, for $\beta > 0$ and $\beta - \omega > 0$ we see that the parameters behave as $w_{eff}(Q_i^+) \rightarrow -\infty$ and $q(Q_i^+) \rightarrow -\infty$, also describing Big Rip singularities.

For $i = 7, 8$ we have $w_{eff}(Q_i^+) \simeq \frac{\beta\omega(16\beta+\mu^2\omega)}{(\rho-1)(16\beta^2+\mu^2\omega^2)} - \frac{16\beta}{\sqrt{1-\rho}\sqrt{24\beta^2+\frac{3\mu^2\omega^2}{2}}}$, $q(Q_i^+) \simeq \frac{3\beta\omega(16\beta+\mu^2\omega)}{(\rho-1)(32\beta^2+2\mu^2\omega^2)} + \frac{1}{\sqrt{\rho-1}}$. For these points, the parameters behave as $w_{eff} = q(Q_i^+) \rightarrow (-\infty)\beta\omega(16\beta+\mu^2\omega)$ they describe Big Rip singularities.

For the final two points, that is $i = 9, 10$ we have $w_{eff}(Q_i^+) \simeq \frac{\beta\lambda^2+\mu^2\omega}{(\rho-1)(-4\beta\lambda+\lambda^2+\mu^2(\omega+1))}$, and $q(Q_i^+) \simeq \frac{3(\beta\lambda^2+\mu^2\omega)}{2(\rho-1)(-4\beta\lambda+\lambda^2+\mu^2(\omega+1))}$ they behave as $w_{eff}(Q_i^+) = q(Q_i^+) \rightarrow (-\infty)(\beta\lambda^2+\mu^2\omega)$ they also describe Big Rip singularities.

The results of this Section are summarized in Table II. Moreover, in Figs. 12, 13, 14, 15, 16, we present two-dimensional phase-portraits at the infinity, that is, for $\rho \rightarrow 1$, and the same behaviour is shown in the right hemisphere of the Poincaré sphere for different values of the free parameters.

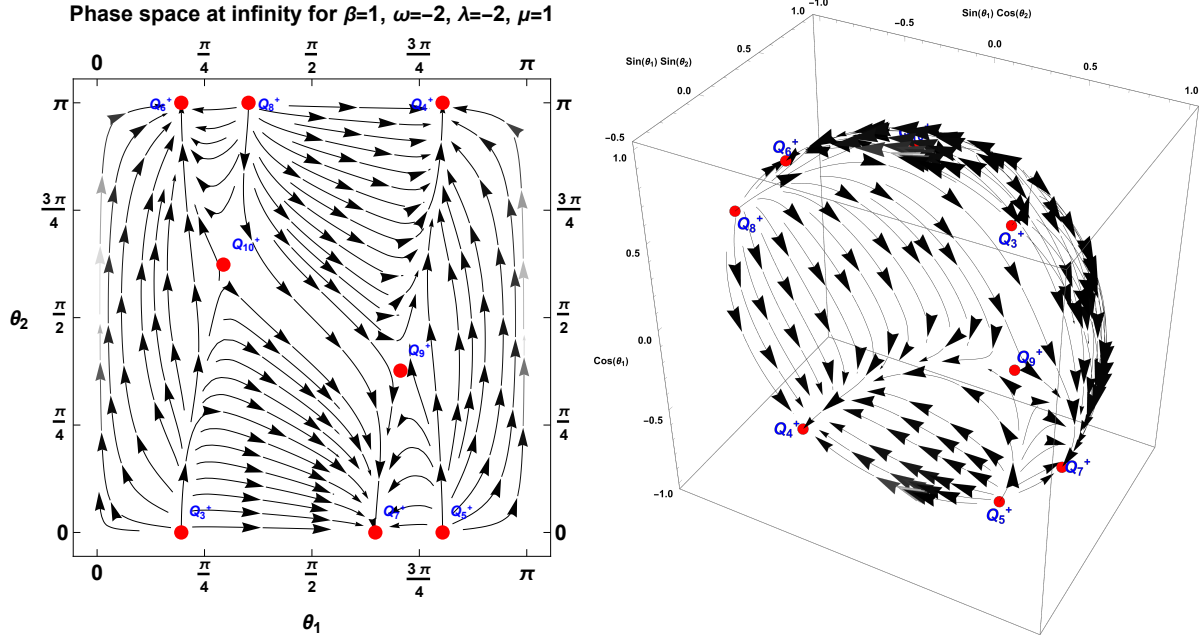


FIG. 12: Eight points exist for this choice of parameters. Left: two-dimensional dynamics at infinity ($\rho \rightarrow 1$). Right: The same behaviour is represented in the right hemisphere of the Poincaré sphere.

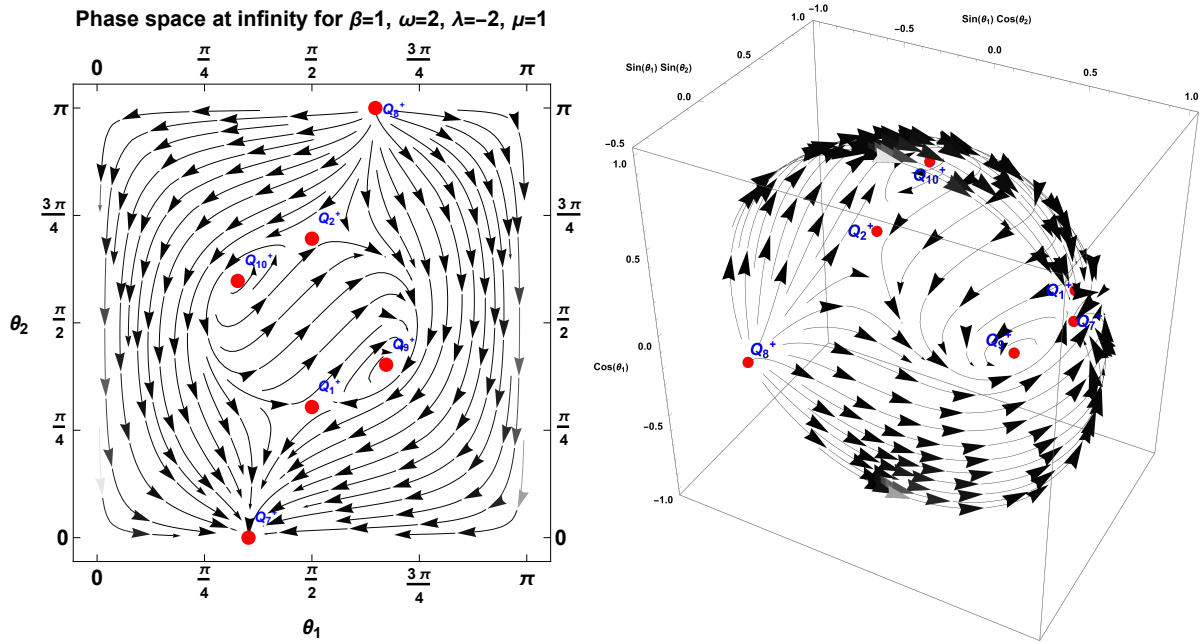


FIG. 13: Six points exist for this choice of parameters. Left: two-dimensional dynamics at infinity ($\rho \rightarrow 1$). Right: The same behaviour is represented in the right hemisphere of the Poincaré sphere.

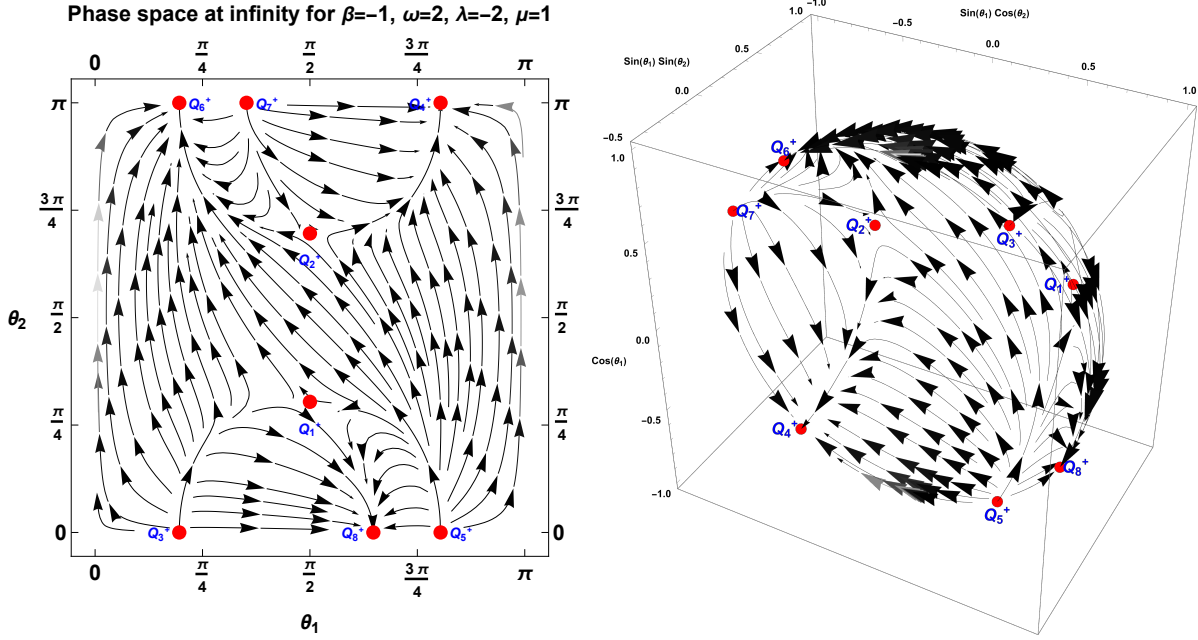


FIG. 14: Eight points exist for this choice of parameters. Left: two-dimensional dynamics at infinity ($\rho \rightarrow 1$). Right: The same behaviour is represented in the right hemisphere of the Poincaré sphere.

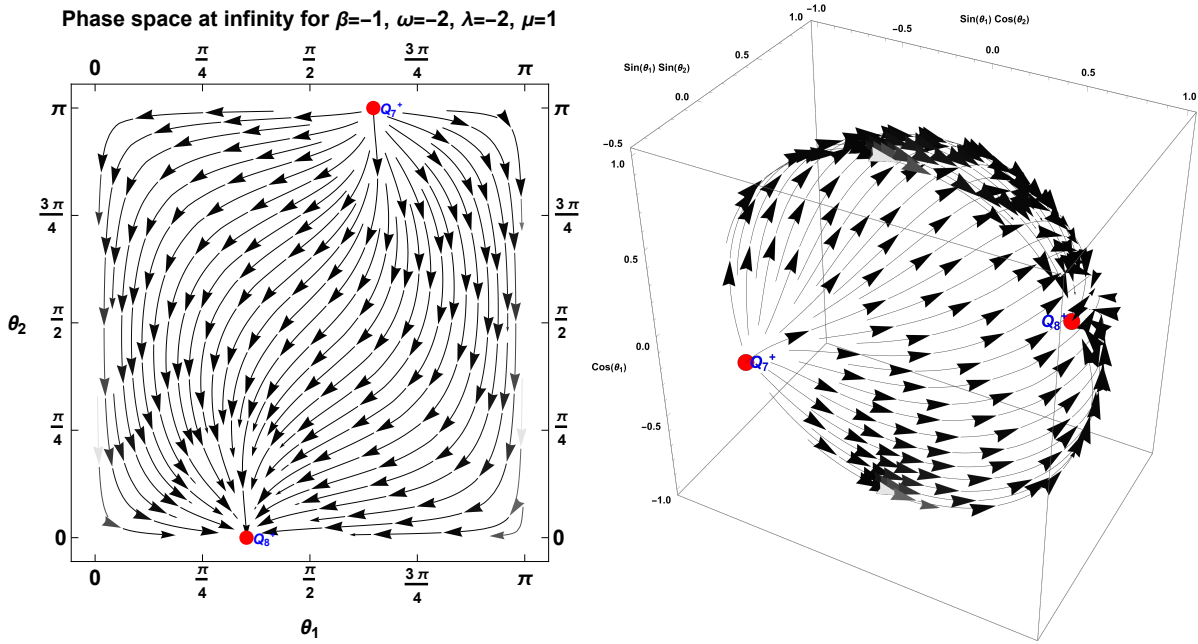


FIG. 15: Two points exist for this choice of parameters. Left: two-dimensional dynamics at infinity ($\rho \rightarrow 1$). Right: The same behaviour is represented in the right hemisphere of the Poincaré sphere.

TABLE II: equilibrium points for the multi-torsion cosmological model in the infinity.

Points	Existence	Attractor?	w_{eff}	q	Acceleration
Q_1^+	see text	No	$-\infty$	$-\infty$	Big Rip
Q_2^+	see text	No	$-\infty$	$-\infty$	Big Rip
Q_3^+	see text	No	$-\infty$	$-\infty$	Big Rip
Q_4^+	see text	No	$-\infty$	$-\infty$	Big Rip
Q_5^+	see text	No	$-\infty$	$-\infty$	Big Rip
Q_6^+	see text	No	$-\infty$	$-\infty$	Big Rip
Q_7^+	see text	Yes	$(-\infty)\beta\omega(16\beta + \mu^2\omega)$	$(-\infty)\beta\omega(16\beta + \mu^2\omega)$	Big Rip
Q_8^+	see text	Yes	$(-\infty)\beta\omega(16\beta + \mu^2\omega)$	$(-\infty)\beta\omega(16\beta + \mu^2\omega)$	Big Rip
Q_9^+	see text	No	$(-\infty)(\beta\lambda^2 + \mu^2\omega)$	$(-\infty)(\beta\lambda^2 + \mu^2\omega)$	Big Rip
Q_{10}^+	see text	No	$(-\infty)(\beta\lambda^2 + \mu^2\omega)$	$(-\infty)(\beta\lambda^2 + \mu^2\omega)$	Big Rip

6. CONCLUSIONS

In this study, we explore the dynamic evolution of physical parameters within a multi-scalar gravitational model, specifically in the context of teleparallelism. Our investigation focuses on the interaction between two scalar fields that are nonminimally coupled to gravity. By considering a spatially flat FLRW background and exponential potentials for the scalar fields, we express the field equations as a three-dimensional first-order dynamical system.

By analyzing this system, we determine the phase space to reconstruct the cosmological evolution and understand the history of the physical parameters. Our analysis involves identifying the equilibrium points and examining the properties and stability of the corresponding asymptotic solutions.

This particular gravitational model is an extension of the Quintom theory within teleparallelism. The equation of the state parameter can cross the phantom-divide line and the future attractor to provide a universe with a deceleration parameter with a value less than minus one. There are equilibrium points corresponding to asymptotic solutions that describe Big Rip singularities, but these points always act as sources or saddle points. The Big Rip singularities are in the past and describe the very early universe. However, there are also attractors that can explain the present or past acceleration of the universe. Other equilibrium

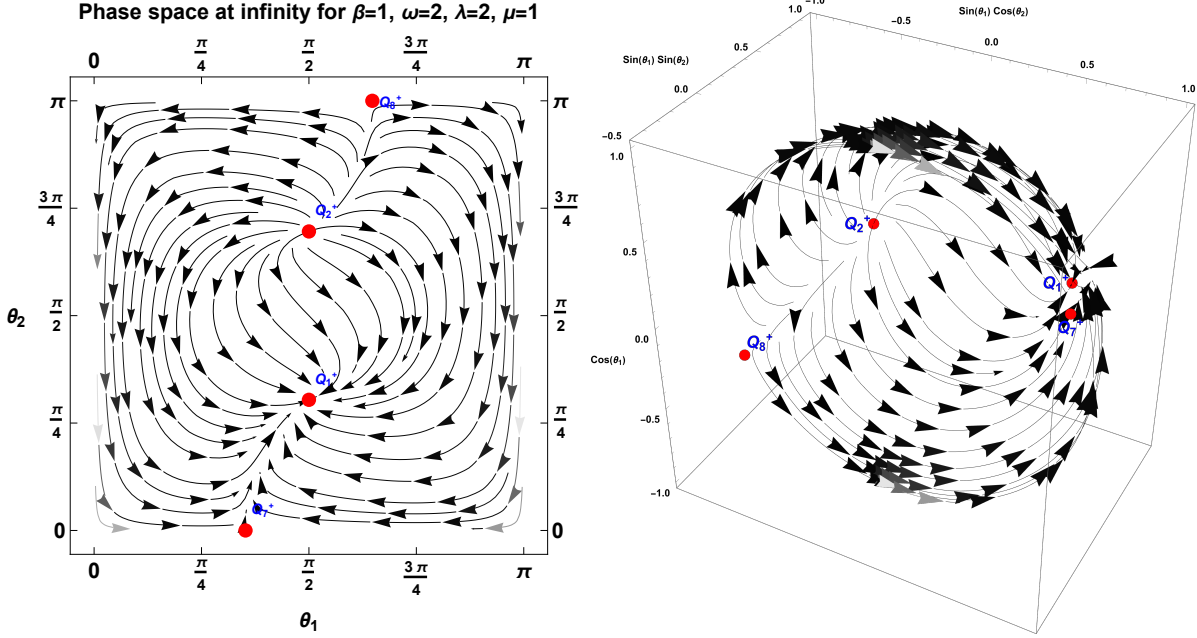


FIG. 16: Four points exist for this choice of parameters. Left: two-dimensional dynamics at infinity ($\rho \rightarrow 1$). Right: The same behaviour is represented in the right hemisphere of the Poincaré sphere.

points can represent different eras in cosmological history. Therefore, this gravitational theory provides a framework to unify the components of the dark sector of the universe. These results extend the previous studies of one scalar field [69, 70], while new equilibrium points exist where the two scalar fields contribute. The two scalar fields can describe not only acceleration eras of the universe but also attribute other matter components, such as dark matter or radiation, from specific values of the free parameters. For instance, there exists the case where P_2 or P_3 can describe a matter-dominated universe.

On the other hand, introducing a matter component minimally coupled to the scalar fields will not affect the general behaviour of these equilibrium points. Additionally, to the previous points, new points which describe the matter are introduced. In this regard, we are looking at the universe's behaviour with respect to its scale factor $a(t)$ under different conditions. When the dark energy equation of state (w_{eff}) is not equal to -1 , the universe's asymptotic solutions have a power-law scale factor: $a(t) = a_0 t^{\frac{2}{3(1+w_{eff})}}$. However, when $w_{eff} = -1$, the universe is described by the de Sitter solution with $a(t) = a_0 e^{H_0 t}$.

To better understand the cosmological history, we also study the stability properties of the equilibrium points. An equilibrium point that is an attractor indicates that the asymptotic solution is stable, while source and saddle points provide unstable solutions. We analyze the

stability of these equilibrium points to extract information related to the stability properties of the exact cosmological solutions derived before. We have investigated the evolution of w_{eff} and q evaluated at a numerical solution of equations (35), (36), and (37) with initial conditions near P_2 . Specifically, we took $x(0) = \frac{\lambda+4}{\sqrt{3\omega}} + 0.1$, $y(0) = \frac{\sqrt{(\lambda+4)^2+3\omega}}{\sqrt{3}\sqrt{\omega}} + 0.1$, and $z(0) = 0.1$. Our analysis shows that for early time, $w_{eff} > -\frac{1}{3}$ and $q > 0$; therefore, there is an early-time deceleration phase. Later, the evolution enters a matter-dominated phase when $w_{eff} = 0$ and $q = \frac{1}{2}$. Quickly after that, the behaviour describes late-time acceleration for $w_{eff} < -\frac{1}{3}$ and $q < 0$. There is also a transient de Sitter behaviour that occurs when both w_{eff} and q cross the value of -1. Finally, they cross to the phantom regime $w_{eff} < -1$ and $q < -1$ with a transient damped oscillation in both parameters.

We used the Poincaré method to extend our study and complete the phase space analysis. We calculated w_{eff} and q at the points Q_i^+ at infinity. For Q_1^+ and Q_2^+ , $w_{eff}(Q_i^+) \simeq \frac{\omega}{(\rho-1)(\omega+1)}$ and $q(Q_i^+) \simeq \frac{3\omega}{2(\rho-1)(\omega+1)}$ behave as $w_{eff}(Q_i^+) \rightarrow (-\infty)\omega$, $q(Q_i^+) \rightarrow (-\infty)\omega$ for $i = 1, 2$. Therefore, these points describe Big Rip singularities. For points $i = 3, 4, 5, 6$ we have $w_{eff}(Q_i^+) \simeq -\frac{4\sqrt{\frac{2}{3}}\sqrt{\beta}}{\sqrt{1-\rho}\sqrt{\beta-\omega}} - 1$, $q(Q_i^+) \simeq -\frac{2\sqrt{6}\sqrt{\beta}}{\sqrt{1-\rho}\sqrt{\beta-\omega}} - 1$. Clearly, for $\beta > 0$ and $\beta - \omega > 0$ we see that the parameters behave as $w_{eff}(Q_i^+) \rightarrow -\infty$ and $q(Q_i^+) \rightarrow -\infty$, also describing Big Rip singularities. For $i = 7, 8$ we have $w_{eff}(Q_i^+) \simeq \frac{\beta\omega(16\beta+\mu^2\omega)}{(\rho-1)(16\beta^2+\mu^2\omega^2)} - \frac{16\beta}{\sqrt{1-\rho}\sqrt{24\beta^2+\frac{3\mu^2\omega^2}{2}}}$, $q(Q_i^+) \simeq \frac{3\beta\omega(16\beta+\mu^2\omega)}{(\rho-1)(32\beta^2+2\mu^2\omega^2)} + \frac{1}{\sqrt{\rho-1}}$. For these points, the parameters behave as $w_{eff} = q(Q_i^+) \rightarrow (-\infty)\beta\omega(16\beta + \mu^2\omega)$ they describe Big Rip singularities. For the final two points, that is $i = 9, 10$ we have $w_{eff}(Q_i^+) \simeq \frac{\beta\lambda^2+\mu^2\omega}{(\rho-1)(-4\beta\lambda+\lambda^2+\mu^2(\omega+1))}$, and $q(Q_i^+) \simeq \frac{3(\beta\lambda^2+\mu^2\omega)}{2(\rho-1)(-4\beta\lambda+\lambda^2+\mu^2(\omega+1))}$ they behave as $w_{eff}(Q_i^+) = q(Q_i^+) \rightarrow (-\infty)(\beta\lambda^2 + \mu^2\omega)$ they also describe Big Rip singularities. To obtain these results, it is necessary to proceed with Poincaré compactification. In Figs. 12, 13, 14, 15, 16, we present two-dimensional phase portraits at infinity, i.e., when $\rho \rightarrow 1$. The same pattern is shown in the right hemisphere of the Poincaré sphere for various values of the free parameters.

Although the dynamical analysis in a finite regime is complete, it can be extended to cases where the Hubble parameter (H) becomes zero. This is because, in some theories, the Hubble parameter changes sign during cosmic evolution and necessarily crosses zero. In such cases, the dynamical variables blow up. In our analysis, we considered $H \neq 0$, and worked on the branch where $H > 0$. However, to consider the case where $H = 0$, we need to normalize the dynamical variables with the quantity $\sqrt{1+H^2}$. This introduces a new

variable and increases the dimension of the dynamical system. As the dimension of the dynamical system is already large, we chose to work with the H -normalization approach. Nonetheless, we can use alternative methods as described in [87, 88] to analyze the dynamics of gravitational field equations like the Chiral-Quintom theory in a Friedman-Lemaître-Robertson-Walker cosmology with an additional matter source. These methods allow us to study both contracting and expanding universes and to investigate a class of bouncing cosmologies where problems with H -normalization typically arise. These methods can help explore the two periods of inflation related to the Universe's early and late-time acceleration phases and the bouncing behaviour.

In this study, we have focused solely on the case of exponential potentials. However, in future research, we intend to expand upon this work by considering more general forms of potential functions. Additionally, we acknowledge the importance of investigating the evolution of cosmological perturbations in this background model, and this aspect will be a subject of interest in our future studies.

Acknowledgments

G. L. was funded by Vicerrectoría de Investigación y Desarrollo Tecnológico (VRIDT) at Universidad Católica del Norte through Resolución VRIDT No. 026/2023 and Resolución VRIDT No. 027/2023 and the support of Núcleo de Investigación Geometría Diferencial y Aplicaciones, Resolución Vridt No. 096/2022. He also acknowledges the financial support of Proyecto de Investigación Pro Fondecyt Regular 2023, Resolución VRIDT No. 076/2023. A. P. thanks the support of VRIDT through Resolución VRIDT No. 096/2022, Resolución VRIDT No. 098/2022. A. D. Millano was supported by ANID Subdirección de Capital Humano/Doctorado Nacional/año 2020 folio 21200837, Gastos operacionales proyecto de tesis/2022 folio 242220121, and VRIDT-UCN.

-
- [1] A.G. Riess et al., *Astron. J.* 116, 1009 (1998)
 - [2] M. Tegmark et al., *Astrophys. J.* 606, 702 (2004)
 - [3] M. Kowalski et al., *Astrophys. J.* 686, 749 (2008)
 - [4] E. Komatsu et al., *Astrophys. J. Suppl. Ser.* 180, 330 (2009)

- [5] N. Suzuki et. al., *Astrophys. J.* 746, 85 (2012)
- [6] Planck Collaboration: Y. Akrami et al., *A&A* 641, A10 (2020)
- [7] A. Guth, *Phys. Rev. D* 23, 347 (1981)
- [8] A.D. Linde, *Phys. Lett. B* 129, 177 (1983)
- [9] A.R. Liddle, *Phys. Lett. B* 220, 502 (1989)
- [10] J.D. Barrow, *Phys. Rev. D* 48, 1585 (1993)
- [11] J.D. Barrow and P. Saich, *Class. Quantum Grav.* 10, 279 (1993)
- [12] R. Kallosh and A. Linde, *JCAP* 13, 027 (2013)
- [13] S. Basilakos and J.D. Barrow, *Phys. Rev. D* 91, 103517 (2015)
- [14] J.D. Barrow and A. Paliathanasis, *Phys. Rev. D* 94, 083518 (2016)
- [15] J. Martin, C. Ringeval and V. Vennin, *Phys. Dark Univ.* 5, 75 (2014)
- [16] B. Ratra and P. J. E. Peebles, *Phys. Rev. D* 37, 3406 (1988)
- [17] J. D. Barrow and P. Saich, *Class. Quant. Grav.* 10, 279 (1993)
- [18] R. R. Caldwell, R. Dave, and P.J. Steinhardt, *Phys. Rev. Lett.*, 80, 1582 (1998)
- [19] P. J. Peebles and B. Ratra, *Rev. Mod. Phys.*, 75, 559, (2003)
- [20] H. K. Jassal, J.S. Bagla, T. Padmanabhan, *Phys. Rev. D* 72 103503, (2005)
- [21] H.K. Jassal, J.S. Bagla, T. Padmanabhan, *Mon. Not. Roy. Astron. Soc. Letters* 356, L11-L16, (2005)
- [22] J.Q. Xia, H. Li, G.B. Zhao and X. Zhang, *Phys. Rev. D* 78, 083524, (2008)
- [23] G.B. Zhao, J.Q. Xia, B. Feng, X. Zhang, *Int. J. Mod.Phys. D* 16 1229, (2007)
- [24] J. Simon, L. Verde, R. Jiménez, *Phys. Rev. D* 71, 123001, (2005)
- [25] W. Liu, J. Ouynag and H. Yang, *Commun. Theor. Phys.* 63, 391 (2015)
- [26] C. Rubano and J.D. Barrow, *Phys. Rev. D* 64, 127301 (2001)
- [27] J.C. Fabris, T.C. da C. Guio, M.H. Daouda and O.F. Piatella, 17, 259 (2011)
- [28] J.D. Barrow and A. Paliathanasis, *Phys. Rev. D* 94, 083518 (2016)
- [29] A. Al Mamon, A. Paliathanasis and S. Saha, *Eur. Phys. J. C* 82, 232 (2021)
- [30] M.C. Bento, O. Bertolami and A.A. Sen, *Phys. Rev. D* 70, 083519 (2004)
- [31] S. Basilakos, G. Lukes-Gerakopoulos, *Phys. Rev. D* 78, 083509 (2008)
- [32] V. Faraoni, *Int. J. Mod. Phys. D* 11, 471 (2002)
- [33] R. R. Caldwell, M. Kamionkowski, and N. N. Weinberg, *Phys. Rev. Lett.* 91, 071301 (2003)
- [34] G. Izquierdo and D. Pavon, *Phys. Lett. B* 639, 1 (2006)

- [35] R.C. Caldwell, M. Kamionkowski and N.N. Weinberg, *P Phys. Rev. Lett.* 91, 071301 (2003)
- [36] J. Khoury and A. Wetlman, *Phys. Rev. Lett.* 93, 171104 (2004)
- [37] J. Khoury and A. Wetlman, *Phys. Rev. D* 69, 044026 (2004)
- [38] J.M. Salim and S.L. Sautú, *Class. Quantum Grav.* 13, 353 (1996)
- [39] L. Amendola, *Phys. Rev. D* 62, 043511 (2000)
- [40] V. Faraoni, *Cosmology in Scalar-Tensor Gravity*, *Fundamental Theories of Physics* vol. 139, Kluwer Academic Press: Netherlands, (2004)
- [41] C. Brans and R. H. Dicke, *Phys. Rev.* 124, 925 (1961)
- [42] S. Carloni, E. Elizalde and S. Odintsov, *Gen. Rel. Gravit.* 42, 1667 (2010)
- [43] M. Postma and M. Volponi, *Phys. Rev. D* 90, 103516 (2014)
- [44] G. Allemandi, M. Capone, S. Capozziello, M. Francaviglia, *Gen. Rel. Grav.* 38, 33 (2006)
- [45] G. W. Horndeski, *Int. J. Theor. Phys.* 10, 363 (1974)
- [46] J. O’Hanlon, *Phys. Rev. Lett.* 29, 137 (1972)
- [47] A. Nicolis, R. Rattazzi and E. Trincherini, *Phys. Rev. D* 79, 064036 (2009)
- [48] C. Deffayet, G. Esposito-Farese and A. Vikman, *Phys. Rev. D* 79, 084003 (2009)
- [49] A.D. Milano, G. Leon and A. Paliathanasis, *Mathematics* 6, 1408 (2011)
- [50] L.P. Chimento, M.I. Forte, R. Lazkoz and M.G. Richarte, *Phys. Rev. D* 79, 043502 (2009)
- [51] J. Socorro, O.E. Nunez, *Eur. Phys. J. Plus* 132, 168 (2017)
- [52] D. Benisty and E.I. Guendelman, *Class. Quantum Grav.* 36, 095001 (2019)
- [53] A. Paliathanasis and G. Leon, *Eur. Phys. J. Plus* 137, 165 (2022)
- [54] A. Paliathanasis, *Class. Quantum Grav.* 37, 19 (2020)
- [55] S Nojiri, SD Odintsov and VK Oikonomou, *Phys. Rep.* 692, 1 (2017)
- [56] T. Clifton, P.G. Ferreira, A. Padilla and C. Skordis, *Phys. Rep.* 513, 1 (2012)
- [57] J. Beltrán-Jiménez, L. Heisenberg and T.S. Koivisto, *Universe* 5, 173 (2019)
- [58] R. Weitzenböck, Nordhoff, Groningen (1923)
- [59] L. Combi and G.E. Romero, *Annalen der Physik* 530, 1700175 (2018)
- [60] K. Hayashi and T. Shirafuji, *Phys. Rev. D* 19, 3524 (1979)
- [61] M. Skugoreva, E.N. Saridakis and A. Toporensky, *Phys. Rev. D* 91, 044023 (2015)
- [62] H. Motavalli and E. Nouri, *Int. J. Mod. Phys. D* 31, 2250061 (2022)
- [63] A. Paliathanasis, *Eur. Phys. J. Plus* 136, 674 (2021)
- [64] A. Paliathanasis, *Mod. Phys. Lett. A* 37, 2250167 (2022)

- [65] H. Wei, Phys. Lett. B 712, 430 (2012)
- [66] G. Otalora, JCAP 07, 044 (2013)
- [67] R. D'Agostino and O. Luongo, Phys. Rev. D 98, 124013 (2018)
- [68] C.-Q. Geng, C.-C. Lee, E.N. Saridakis and Y.-P. Wu, Phys. Lett. B 704, 34 (2017)
- [69] C. Xu, E.N. Saridakis and G. Leon, JCAP 07, 005 (2012)
- [70] L. Järv and J. Lember, Universe 7, 179 (2021)
- [71] M. Skugoreva, E.N. Saridakis and A. Toporensky, Phys. Rev. D 91, 044023 (2015)
- [72] L. Järv and A. Toporensky, Phys. Rev. D 93, 024051 (2016)
- [73] H.M. Sadjadi, Phys. Rev. D 92, 12353 (2015)
- [74] M. Skugoreva, Gravit. Cosm. 24, 103 (2018)
- [75] H.M. Sadjadi, JCAP 01, 031 (2017)
- [76] M. Hohmann, L. Järv and U. Ualikhanova, Phys. Rev. D 97, 104011 (2018)
- [77] M. Hohmann, L. Järv, P. Kuusk, E. Randla and O. Vilson, Phys. Rev. D 94, 124015 (2016)
- [78] K. Dialektopoulos, G. Leon and A. Paliathanasis, Eur. Phys. J. C 83, 218 (2023)
- [79] L. Amendola, D. Polarski and S. Tsujikawa, Phys. Rev. Lett. 98, 131302 (2007)
- [80] L. Amendola, R. Gannouji, D. Polarski and S. Tsujikawa, Phys. Rev. D 75, 083504 (2007)
- [81] A. Coley and G. Leon, Gen. Rel. Grav. 51, 115 (2019)
- [82] B.-F. Li, P. Singh and A. Wang, Qualitative dynamics and inflationary attractors in loop cosmology, Phys. Rev. D 98, 066016 (2018)
- [83] L. Chen, Dynamical analysis of loop quantum R^2 cosmology, Phys. Rev. D 99, 064025 (2019)
- [84] T. Gonzalez, G. Leon and I. Quiros, Class. Quantum Grav. 23, 32165 (2006)
- [85] P. Christodoulidis, D. Roest and E.I. Sfakianakis, JCAP 12, 059 (2019)
- [86] E.J. Copeland, A.R. Liddle and D. Wands, Phys. Rev. D 57, 4686 (1998)
- [87] G. Leon, A. Coley, A. Paliathanasis, J. Tot and B. Yildirim, [arXiv:2308.02470 [gr-qc]]
- [88] J. Tot, B. Yildirim, A. Coley and G. Leon, Phys. Dark Univ. **39** (2023), 101155